# Generation separation in simple structured life-cycles: models and 48 years of field data on a tea tortrix moth

# Generation separation in simple structured life-cycles: models and 48 years of field data on a tea tortrix moth[†]

Takehiko Yamanaka[1], William A. Nelson[2], Koichiro Uchimura[3], and Ottar N. Bjørnstad[4]

*Accepted September 6, 2011*

[1] Biodiversity Division, National Institute for Agro-Environmental Sciences, 3-1-3 Kannondai, Tsukuba, Ibaraki 305-8604, Japan
[2] Department of Biology, Queen's University, Kingston, Ontario, K7L 3N6, Canada
[3] Kagoshima Tea Experiment Station, 3964 Nagasato Chiran-cho (Kawabe county) Kagoshima, 897-0303, Japan
[4] Departments of Entomology and Biology, 501 Ag Sciences and Industries Building, The Pennsylvania State University, University Park, PA 16802, U.S.A.

## ABSTRACT

Population cycles have fascinated ecologists since the early 19th century, and dynamics of insect populations have been central to understanding the intrinsic and extrinsic biological processes responsible for these cycles. We analyzed an extraordinary long-term dataset (every 5 days for 48 years) of a tea tortrix moth (*Adoxophyes honmai*) which exhibits two dominant cycles: a conspicuous 4-5 single-generation cycles in a year superimposed on an annual cycle. General theory offers several candidate mechanisms for generation cycles. To evaluate these we construct and parameterize a series of temperature dependent stage-structured models that includes intraspecific competition, parasitism, mate-finding Allee effects and adult senescence, all in the context of a seasonal environment. By comparing the observed dynamics with predictions from the models, we find that even weak larval competition in the presence of seasonal temperature forcing predicts the two cycles accurately. None of the other mechanism predicts the dynamics. Detailed dissection of the results shows that a short reproductive life-span and differential winter mortality among stages are the additional life-cycle characteristics that permits the sustained cycles. Our general modeling approach is applicable to a wide range of organisms with temperature-dependent life-histories, and is likely to prove particularly useful in temperate systems where insect pest outbreaks are both density- and temperature-dependent.

***Keywords:*** Adoxophyes honmai*, delay differential equations, wavelet analysis, stage-structured models, Allee effects*

## INTRODUCTION

Population cycles have fascinated ecologists since the early 19th century (Elton 1924), and dynamics of insect populations have been central to understanding the intrinsic and extrinsic biological processes responsible for these cycles (e.g., Andrewartha & Birch 1954; Nicholson 1954a). Various laboratory systems have been used to study the underlying mechanics of population cycles; famously, the single-generation cycles in the Indian meal moth (Gurney, Blythe, et al. 1980), the overcompensation (2-generation) cycles of Nicholson's blowflies (Gurney, Blythe, et al. 1980; Nicholson 1954b), and the cyclic and chaotic fluctuations in flour beetles (e.g., Costantino et al. 1997) and bruchid beetles (Shimada & Tuda 1996). Wild insects also provide prominent examples of cyclic dynamics, particularly among univoltine (single generation per year) foliage feeders such as the larch budmoth (Baltensweiler 1993), the spruce budworm (Royama et al. 2005), and the pine looper (Kendall et al. 2005). Interestingly, many of the classic cycles observed in natural populations are generated by interspecific interactions (e.g., consumer-resource interactions) rather than by the within- and among-stage intraspecific interactions found in many laboratory populations (Berryman 2002). One consequence is that the population cycles in natural systems tend to have a longer period (relative to their maturation time) than the cycles observed in the lab, as predicted by theory (Murdoch et al. 2002).

In this study, we use the long-term tortrix dataset to investigate the relative importance of regular disturbance from seasonal temperature changes (favored by the empirical entomological literature) versus intra- or interspecific density-dependent interactions (favored by the theoretical literature) in generating the intra-annual single-generation cycles and sustaining the generation separation. We follow the now more-or-less standard protocol in the study of population cycles of combining mechanistic mathematical models with detailed time series analysis (e.g., Bjørnstad & Grenfell 2001; Bjørnstad & Grenfell 2001; Ellner et al. 1998; Ellner et al. 1998). We apply wavelet analysis to the time series to dissect the pattern of periodicity in the data. We then construct a stage-structured population model of a set of delay-differential equations to investigate the genesis of the single-generation cycles (Gurney, Blythe, et al. 1980; Nisbet & Gurney 1983) based on temperature-dependent growth, birth and death rates from laboratory life-cycle experiments. One challenge with this class of models is that simulating dynamics under fluctuating seasonal temperatures means that development rates will vary through time, which introduces time-dependence in the delays. To circumvent this challenge, we use a rescaling-of-time method (McCauley et al. 2008) to transform the time-dependent delay model into a fixed-delay model on a physiological time scale, which allows us to use standard methods to study stability and cyclicity.

## METHODS

The number of adult smaller tea tortrix, *Adoxophyes honmai* Yasuda (Lepidoptera: Tortricidae) caught by a light trap (equipped with a 20W fluorescent lamp and a 1m diameter water pan) was counted every five or six days for 48 years from 1961 to 2008. The monitoring program is carried out by the prefectural researchers to guide pesticide application on commercial farms. Sampling covered the full flight season of the moth from March 1st to November 31st each year (Figure 1). The trap is located on a tea orchard of the Kagoshima Tea Experiment Station, Japan (Chiran township, 31°22'E, 130°26'E). The main tea cultivar planted there is Yabukita (*Camellia sinensis* L. var Yabukita) though there are several other varieties present. Scheduled pest control was routinely conducted with generic organophosphorus insecticides such as fenitrothion (MEP; Sumitomo Chemical, Tokyo, Japan)

[†]This is the accepted version of the following article: Yamanaka T. et al. (2012) *The American Naturalist* 179: 95–109. The final published version is available at: https://doi.org/10.1086/663201.

since the 1960s or granulovirus application since the early 1990s (Nakai 2009). The daily mean temperature used in our study was recorded at the Kagoshima Tea Experiment Station.

## Study System

The smaller tea tortrix, *A. homai*, is a tea leafroller and is one of the major tea pests in Japan. They produce four to five generations per year. Though there are no reports of an obligatory diapause in winter, anything but larvae is rarely seen during the coldest months (Tamaki 1991). Egg, pupal and adult stages suffer high mortality in this period. There are generally five to six larval instars. In our study we aggregated these into two stages (young larvae and old larvae) when investigating asymmetric competition. Larvae inhabit and pupate in nest webs made of one or several young leaves spun together.. Adult moths can live more than two weeks but females ordinary mate and oviposit only during the first half of their adult lives (Nabeta et al. 2005, see also Appendix A). Mating behavior is typically observed in the nights. Male moths find their mates using female emitted sex-pheromones as a cue of sexual communications (Tamaki 1991). As with most insect, both developmental rates and vital rates are highly temperature dependent (Appendix A).

More than 20 parasitoids are reported to forage on eggs and larvae of *A. homai*. *Ascogaster reticulata* (Braconidae) and *Apanteles adoxophyesi* (Braconidae) are the most two abundant wasps throughout Japan (Nakai 2009; Takagi 1974; Yukinari 1976). Roughly speaking, these wasps have life-cycles of the same duration as that of the host (Takagi 1974; Yukinari 1976). For example, the females of *A. reticulata* oviposit on the egg mass of *A.honmai* and only a single adult parasitoid emerges from each parasitized larvae. The fully-developed parasitoid larva emerge from the host to pupate at the outside (Kainoh & Tamaki 1982). Parasitized host larvae continue to feed on tea leaves (Nakai 2009), and wasp emergence is synchronous with host pupation, so we may assume that parasitized eggs and larvae have the same mortality rates as unparasitized hosts.

## Statistical Analysis

We convert the data from a Julian day time-scale to a temperature-based physiological scale because the developmental rate of insects depends on temperature. A common approach in entomology is to scale development rate by cumulative degree-day so as to better predict the timing of pest outbreaks (e.g., Baskerville & Emin 1969; Yamanaka, Tatsuki, et al. 2008). Cumulative degree-days are often calculated by summing the daily temperature for days when the temperature is above the minimum required for development (Roltsch et al. 1999), which implies that development rate i) is a linear function of temperature and ii) falls abruptly to zero at a critical threshold. While cumulative degree-days is a step towards scaling time to a more appropriate development-rate scale based on temperature, it does not fully incorporate the observed response of insect development to temperature. Here we use a transformation that explicitly includes the influence of temperature on development rates in *A. honmai*.

Temperature ($D(t)$) at time $t$ is converted to the physiological scale of the insect using the following empirically-motivated logistic development rate function ($h_i(t)$)

$$h_i(t) = \frac{\alpha_i}{1 + \exp\left(-\gamma_D(D(t) - h_D)\right)} \tag{1}$$

where $h_D$ is the temperature at which the development rate function reaches half the asymptotic value, $\alpha_i$ is a scaling coefficient specific to each stage (e.g., egg, larvae, pupae, adult), and $\gamma_D$ controls the steepness of the function (see Appendix A for full details). The development rate $h_i(t)$ indicates how fast individuals move through the $i$th stage. While alternative functions (e.g., exponential or quadratic) provide a similar fit to the data, we chose the logistic function because it approaches a finite level at high temperatures and approaches zero smoothly at low temperature. The new physiological time scale $\phi(t)$ (hereafter referred to as *phi-scale*) is calculated by integrating the stage-independent (i.e., excluding $\alpha_i$ in eq. (1)) base function

$$g(t) = \frac{1}{1 + \exp\left(-\gamma_D(D(t) - h_D)\right)} \tag{2}$$

according to

$$\phi(t) = \int_0^t g(x)dx \tag{3}$$

The base function $g(t)$ has no direct biological interpretation, but can be used to rescale Julian days into a developmental scale for all stages. Moreover, there is a direct connection between the rescaling used in the data analysis and the rescaling used in the model. Specifically, when $\phi(t_1) - \phi(t_2) = 1/\alpha_i$, then a cohort entering stage $i$ at time $t_1$ will have completed the development through this stage at time $t_2$ (see Appendix A and Appendix B for full details). It should be noted that we only have mean daily temperatures at the study site. As such, estimates of $\phi(t)$ from the field were calculated using the mean daily temperature.

The raw time-series of moth abundance suggests that the tea pest populations cycle at more than one frequency. To decompose the frequency-specific dynamics and how they may change through time, we use wavelet analysis (Carmona et al. 1998; Grenfell et al. 2001; Keitt & Urban 2005; Torrence & Compo 1998). Specifically, we use the Morlet wavelet transformation, which is a complex exponential function with amplitude that is localized by a Gaussian window. The wavelet analysis was done using the *Rwave* library in the R statistical environment (R Development Core Team 2011). Although insect abundance was estimated regularly on the Julian day scale, transformation to the physiological scale results in temporally uneven data that cannot be used directly for wavelet analyses. To conduct the wavelet analysis, we therefore smoothed the abundance data on the phi scale, and resampled it every 1.62 $\phi$, which corresponds to about 100 data points per year. Smoothing was conducted with a flexible cubic smoothing spline ($df = 60$) in the *mgcv* library of R. The global periodogram is shown as the wavelet averaged across time. We used a randomization test on the global periodogram to generate a 99% null envelop under the assumption that the patterns in the time series represents random noise. Peaks in the observed periodogram that extend

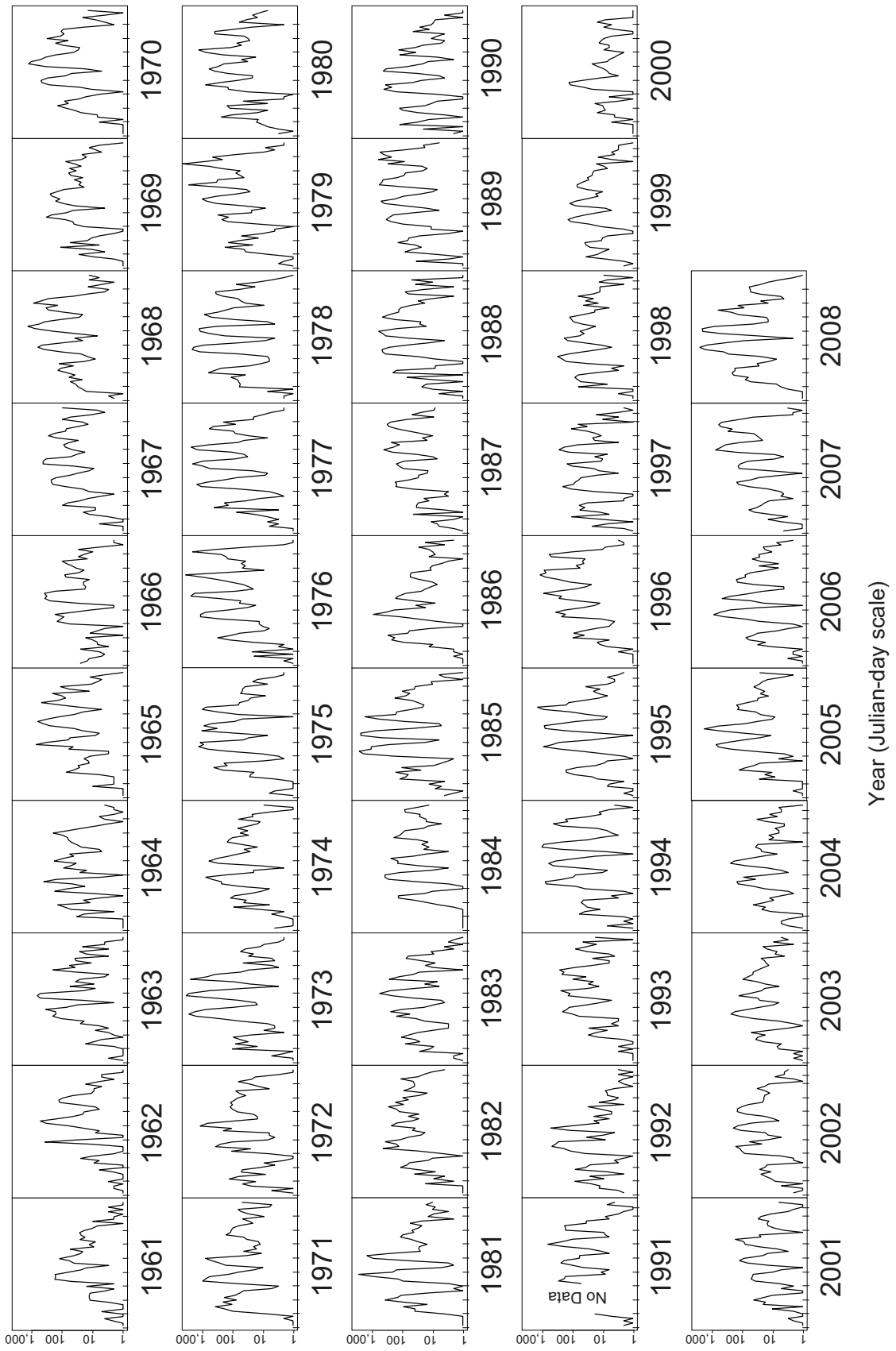


**Figure 1.** Light-trap census of adult tortrix moths (*Adoxophyes honmai*) over 48 years (from March 1 to November 30). Counts are log transformed, and the *X*-axis is measured in Julian days.

outside of this envelope represent statistically non-random patterns at the 1%-level. We used 1,000 permutations for the randomization test.

## Model Development

We consider six plausible ecological mechanisms to explain the strong generation cycle observed in the tortrix moth: i) density-dependence through symmetric intraspecific larval competition, ii) density-dependence through asymmetric intraspecific larval competition, iii) adult senescence, iv) Allee effect due to mate-finding limitation, v) interaction with a parasitoid wasp, and vi) strong winter mortality on egg, pupae and adult stages. As we expand on below, temperature influences all aspects of the moth life-history. The first five mechanisms are ecologically based and assume that all stages respond synchronously to natural variation in temperature. The last mechanism, *winter mortality*, introduces a more realistic temperature effect on mortality that is not synchronous across stages. Here we outline the general model (see Appendix B for full model development), and a series of model variants that incorporate different combinations of these six mechanisms (summarized here and fully developed in Appendix C) for a total of twelve models.

The general model is motivated by the tortrix moth life-cycle, which has five morphologically distinct stages: eggs ($E(t)$), young larvae ($L_1(t)$), old larvae ($L_2(t)$), pupae ($P(t)$) and adults ($A(t)$). Since cohorts of individuals develop through the stages synchronously, the most appropriate modelling framework is delay-differential equations (DDEs), which is similar in structure to many previous models of insect population dynamics (Gurney & Nisbet 1998; Gurney, Nisbet & Lawton 1983; Nisbet 1996; Nisbet & Gurney 1983). While there is some variation among individuals in development time in real populations, our conclusions are robust to the assumption of a fixed stage duration rather than exponential- or gamma-distributed stage durations (see Appendix D).

Parasitism is modelled based on the life cycle of the dominant parasitoid wasp of tortrix moths *A. reticulata*. The number of parasitized moth larvae, young and old, and the number of adult wasps are denoted by $L_1^W(t)$, $L_2^W(t)$ and $W(t)$, respectively. We assume that the stage durations of the wasp match those of their host, such that they share the same developmental rates $\alpha_{L_1}$, $\alpha_{L_2}$ and $\alpha_A$ ($\alpha_P$ for pupa was also assumed implicitly in eq. (4), see Model System). We also assume that parasitism does not affect the mortality rates of the juvenile stages (i.e. $\delta_{L_1}$, $\delta_{L_2}$, and $\delta_P$ are used for parasitized hosts as well).

The development rate through each stage is temperature-dependent (Appendix A), which means that stage durations, and thus the time-delays in the DDEs, fluctuate through time. To make the models more amenable for analysis, we follow McCauley et al. (2008) and transform the model from the time-scale where the delays are variable, to a development rate scale where the delays are fixed (Appendix B). The procedure is analogous to the rescaling done in the statistical analysis of the field data. Defining $\phi(t)$ as the new physiological scale (eq. (2)), the dynamics of egg ($E(\phi)$), larval ($L_1(\phi)$, $L_2(\phi)$), pupal ($P(\phi)$) and adult ($A(\phi)$), parasitized larval ($L_1^W(\phi)$, $L_2^W(\phi)$), and wasp ($W(\phi)$) populations can be modelled in general by:

$$
\begin{aligned}
\frac{dE(\phi)}{d\phi} &= \frac{\beta(\phi)}{m(\phi)}A(\phi) \\
&\quad - \frac{\beta(\phi_E)}{m(\phi_E)}A(\phi_E)S_E(\phi) - \frac{\delta_E(\phi)+\rho_W(\phi)}{m(\phi)}E(\phi) \\
\frac{dL_1(\phi)}{d\phi} &= \frac{\beta(\phi_E)}{m(\phi_E)}A(\phi_E)S_E(\phi) \\
&\quad - \frac{\beta(\phi_{L_1})}{m(\phi_{L_1})}A(\phi_{L_1})S_{L_1}(\phi) - \frac{\delta_{L_1}(\phi)}{m(\phi)}L_1(\phi) \\
\frac{dL_2(\phi)}{d\phi} &= \frac{\beta(\phi_{L_1})}{m(\phi_{L_1})}A(\phi_{L_1})S_{L_1}(\phi) \\
&\quad - \frac{\beta(\phi_{L_2})}{m(\phi_{L_2})}A(\phi_{L_2})S_{L_2}(\phi) - \frac{\delta_{L_2}(\phi)}{m(\phi)}L_2(\phi) \\
\frac{dP(\phi)}{d\phi} &= \frac{\beta(\phi_{L_2})}{m(\phi_{L_2})}A(\phi_{L_2})S_{L_2}(\phi) \\
&\quad - \frac{\beta(\phi_P)}{m(\phi_P)}A(\phi_P)S_P(\phi) - \frac{\delta_P(\phi)}{m(\phi)}P(\phi) \\
\frac{dA(\phi)}{d\phi} &= \frac{\beta(\phi_P)}{m(\phi_P)}A(\phi_P)S_P(\phi) \\
&\quad - \sigma\frac{\beta(\phi_A)}{m(\phi_A)}A(\phi_A)S_A(\phi) - \frac{\delta_A(\phi)}{m(\phi)}A(\phi)
\end{aligned}
$$

$$
\begin{aligned}
\frac{dL_1^W(\phi)}{d\phi} &= \frac{\rho_W(\phi)}{m(\phi)}E(\phi) \\
&\quad - \frac{\rho_W(\phi_{L_1})}{m(\phi_{L_1})}E(\phi_{L_1})S_{L_1}^W(\phi) - \frac{\delta_{L_1}(\phi)}{m(\phi)}L_1^W(\phi) \\
\frac{dL_2^W(\phi)}{d\phi} &= \frac{\rho_W(\phi_{L_1})}{m(\phi_{L_1})}E(\phi_{L_1})S_{L_1}^W(\phi) \\
&\quad - \frac{\rho_W(\phi_{L_2})}{m(\phi_{L_2})}E(\phi_{L_2})S_{L_2}^W(\phi) - \frac{\delta_{L_2}(\phi)}{m(\phi)}L_2^W(\phi) \\
\frac{dW(\phi)}{d\phi} &= \frac{\rho_W(\phi_P)}{m(\phi_P)}E(\phi_P)S_P^W(\phi) - \frac{\delta_W(\phi)}{m(\phi)}W(\phi)
\end{aligned}
$$

$$
\begin{aligned}
S_i(\phi) &= \exp\left(-\sum_{x=E}^{i}\int_{\hat{\phi}_{x:i}}^{\hat{\phi}_{x+1:i}}\frac{\delta_x(\xi)}{m(\xi)}d\xi\right) \\
S_i^W(\phi) &= \exp\left(-\sum_{x=L_1}^{i}\int_{\hat{\phi}_{x:i}}^{\hat{\phi}_{x+1:i}}\frac{\delta_x(\xi)}{m(\xi)}d\xi\right) \\
\phi_i &= \phi - \sum_{x=E}^{i}\frac{1}{\alpha_x} \\
\hat{\phi}_{j:k} &= \begin{cases} \phi - \sum_{x=j}^{k}\frac{1}{\alpha_x} & \text{if } j \le k \\ \phi & \text{if } j > k \end{cases}
\end{aligned}
\tag{4}
$$

Here, $\beta(\phi)$ is the function describing the per-capita birth rate, $\delta_i(\phi)$ is the function describing the instantaneous per-capita mortality rate of stage $i$, and $\rho_W(\phi)$ is the per-capita parasitoid attack rate at $\phi$. The function $m(\phi)$ is the base development rate at the current ($\phi$) or delayed ($\phi_i$) physiological time, where $\phi_i$ is the fixed stage duration from the beginning of the egg stage to the end of stage $i$ ($i \in \{E, L_1, L_2, P, A\}$).

$S_i(\phi)$ is through-stage survivorship from the beginning of the egg stage born at delayed physiological time ($\phi_i$) to stage $i$ at current physiological time ($\phi$). The parameter $\sigma$ is introduced to switch adult senescence on or off, and takes on either a value of one or zero. Though the transformed model appears more complex than the untransformed model (eqq. ($B1$)-($B10$) in Appendix B), it has fixed delays and thus is amenable to analysis using standard mathematical tools to study equilibria and stability. Since the transformation only influences the time-axis, stability and cycle amplitudes are identical for the two scales ($\phi$-scale and time-scale), which allows us to study the time-scale system dynamics using phi-scale models that are easier to characterize. The model given by eq. (4) is the general case for a hierarchy of simplified model variants which we describe in the following sections (Appendix C). These models represent a series of plausible biological hypotheses to explain the cycles. Also, for a number of these model variants, the $m(\phi)$ function cancels out on the phi-scale, which means that the qualitative dynamics of the system do not depend on temperature even though the life-cycle is highly temperature-dependent.

Each model variant is arrived at by specifying a particular form for the birth, death, and parasitism rate functions, along with the accompanying parameters. Table 1 lays out the functions used for each of the biological mechanisms, Table 2 shows the estimated parameter values, and Table 3 shows the model variants studied. The following sections detail the model development for each biological mechanism, and the simplified equations are presented in Appendix C. Model dynamics were characterized through equilibrium stability analysis and numerical simulations. Numerical simulations were done using the *PBSddesolve* library in R, and run for $\phi = 1,616$ units (corresponding to roughly ten years) to reach asymptotic dynamics. Cycle period was estimated from the last $\phi = 808$ units (corresponding to five years). All simulations were started with an adult inoculation that mimics the emergence of overwintering moths in early spring (Gaussian distribution with mean =11.3 and sd= 2.2 on the $\phi$-scale).

## Model Variants

The life-history data for tortrix moths suggest that, in the absence of larval density-dependence, birth and death rates are strongly temperature-dependent in a manner similar to the development rate (Nabeta et al. 2005, Appendix A). As such, we define the base birth and mortality rate functions as $\beta(\phi) = cm(\phi)$ and $\delta_i(\phi) = n_i m(\phi)$ respectively, where $c$ is a constant birth rate scalar and $n_i$ is a stage-specific constant mortality rate scalar. Stage-specific development rate functions are given by $h_i(\phi) = \alpha_i m(\phi)$, where $\alpha_i$ is the stage-specific development rate scalar. This base model is density independent, and thus an unrealistic description for a system with a well defined seasonal mean abundance. However, these functions describe the basic structured moth life-history in the absence of the candidate density-dependent interactions and serves as the point of departure for a series of models.

**Symmetric Intraspecific Larval Competition:** Direct competition is only among larval stages of the tortrix tea pest because this is the only stage that feeds. In this model variant (Model A), larval mortality is uniformly density-dependent as young and old larvae are assumed interchangeable in their mutual competitive reduction of survivorship. The intensity of competition, whether through increased feeding or metabolic rates, is assumed temperature dependent We further assume a Lotka-Volterra formulation for competition (according to Briggs et al. 2000) that scales with temperature, which results in a larval mortality rate given by $\delta_{L_1} = \delta_{L_2} = (n_L + n_C L(\phi))m(\phi)$, where $L(\phi) = L_1(\phi) + L_2(\phi)$, $n_L$ is the base density-independent mortality rate, and $n_C$ controls the increase in mortality due to larval density-dependence. To study how the strength of larval density-dependence alters the system dynamics, we simulate dynamics over a range of birth rates from $c = 0$ to $c = 30$. It should be noted that changes in $c$ influence the strength of density-dependence through changing the density of larvae, while changing the density-dependent scalar $n_C$ has no influence on model dynamics. We use $n_C = 1 \times 10^{-6}$ for the simulations, which generates cycles with amplitude similar to the observed dynamics.

**Asymmetrical Intraspecific Larval Competition:** Previous theoretical work has shown that asymmetrical larval density-dependence (either through competition or cannibalism) can generate generation cycles in other insects (e.g., Gurney, Nisbet & Lawton 1983; Briggs et al. 2000), though there is no particular empirical evidence for this in tortrix moths. We investigate this mechanism by assuming that the larval stage can be divided into young ($L_1(\phi)$) and old larval stages ($L_2(\phi)$) at the mid-point of the stage, that the development rate is the same for both stages, and that the total larval development time ($\alpha_L$) remains unchanged (i.e., $1/\alpha_{L_1} = 1/\alpha_{L_2}$). We define the strength of asymmetry ($\psi$) as the competitive effect of old larvae on young larvae. Assuming that the competitive effect of young on old larvae is the inverse of $\psi$, we can write the larval mortality functions as $\delta_{L_1} = (n_L + n_C(L_1(\phi) + \psi L_2(\phi)))m(\phi)$ and $\delta_{L_2} = (n_L + n_C(\frac{L_1(\phi)}{\psi} + L_2(\phi)))m(\phi)$, respectively.

**Adult Senescence:** The life-history experiments provide strong evidence for senescence in reproductive females (Briggs et al. 2000; Nabeta et al. 2005, see also Appendix A), which we incorporate by assuming a fixed duration of the adult life-span (using the same fixed-delay structure as recruitment through the immature stages). In equations (4), this is done by setting $\sigma = 1$. Since this mechanism is density-independent if it is not combined with some other density-dependent factor, it will never prevent population from an unrealistic growth explosion or an abrupt extinction. Thus, we incorporate this in combination with some form of larval density-dependence.

**Mate-finding Allee Effect:** While there is no empirical evidence for an Allee effect in tortrix moths, it provides a possible explanation for sustaining cycles and generation separation (Srinivasa & Muralimohan 2008). A mate-finding Allee effect is common in many other lepidopteran pests (Yamanaka & Liebhold 2009). We incorporate this into the model using the structure described by Dennis (1989). Specifically, the probability of a female finding a male searching in area $\mu$ is $1 - \exp(\nu A(\phi))$, which yields a new birth rate function $\beta(\phi) = c\,(1 - \exp(\nu A(\phi)))\,m(\phi)$. To evaluate the impact of an Allee effect on the predicted dynamics, we consider values of $\nu$ from $\nu = 0.0001$ to $\nu = 1.0$. As with senescence, this mechanism is not negatively density-dependent; we thus only consider it in combination with a form of larval density-dependence.

**Table 1.** Function definition for proposed biological mechanisms

| Mechanism[a] | $\beta/m$ | $\delta_E/m$ | $\delta_A/m$ | $\rho_W/m$ | $\delta_{L_1}/m$ | $\delta_{L_2}/m$ | $\delta_P/m$ | $\sigma$ |
|---|---|---|---|---|---|---|---|---|
| Base | $c$ | $n_E$ | $n_A$ | 0 | $n_L$ | $n_L$ | $n_P$ | 0 |
| SLDD | $c$ | $n_E$ | $n_A$ | 0 | $n_L + n_C L$ | $n_L + n_C L$ | $n_P$ | 0 |
| ALDD | $c$ | $n_E$ | $n_A$ | 0 | $n_L + n_C(L_1 + \psi L_2)$ | $n_L + n_C(L_1/\psi + L_2)$ | $n_P$ | 0 |
| Sen. | $c$ | $n_E$ | $n_A$ | 0 | $n_L + n_C L$ | $n_L + n_C L$ | $n_P$ | 1 |
| Allee | $c(1 - e^{\nu A})$ | $n_E$ | $n_A$ | 0 | $n_L + n_C L$ | $n_L + n_C L$ | $n_P$ | 0 |
| W mort | $c$ | $n_E + n_{q_1} e^{-n_{q_2} m}/m$ | $n_A + n_{q_1} e^{-n_{q_2} m}/m$ | 0 | $n_L + n_C L$ | $n_L + n_C L$ | $n_P + n_{q_1} e^{-n_{q_2} m}/m$ | 0 |
| Para | $c$ | $n_E$ | $n_A$ | $k \ln(1 - uW/k)$ | $n_L$ | $n_L$ | $n_P$ | 0 |

Note that rates are scaled by $m(\phi)$.
SLDD: symmetric larval competition; ALDD: asymmetric;
Sen: senescence; Allee: mate limitation; W mort: winter mortality; Para: parasitoid. $L = L_1 + L_2$.

**Table 2.** Model parameters

| Symbol | Description | Value [Range] | Source |
|---|---|---|---|
| $\gamma_D$ | Steepness parameter in base physiological scale function | 0.258 | Appendix A |
| $h_D$ | Half-saturation parameter in base physiological scale function | 18.6 | Appendix A |
| $\alpha_E$ | Egg stage development scalar | 0.184 | Appendix A |
| $\alpha_{L_1}, \alpha_{L_1 2}$ | Larval stage development scalar | 0.148 | Appendix A |
| $\alpha_P$ | Pupal stage development scalar | 0.198 | Appendix A |
| $\alpha_A$ | Adult stage development scalar (i.e., senescence) | 0.149 | Appendix A |
| $n_E$ | Egg stage mortality scalar | $6.32\times10^{-2}$ | Appendix A |
| $n_{L_1}, n_{L_2}$ | Larval stage mortality scalar | $2.57\times10^{-3}$ | Appendix A |
| $n_P$ | Pupal stage mortality scalar | $2.02\times10^{-2}$ | Appendix A |
| $n_A$ | Adult stage mortality scalar | $8.07\times10^{-2}$ | Appendix A |
| $n_C$ | Density-dependent larval mortality scalar | $1\times10^{-6}$ | Methods |
| $n_{q_1}$ | Temperature mortality scalar | 20 | Methods |
| $n_{q_2}$ | Temperature mortality response | 0.45 | Methods |
| $c$ | Maximum per-capita birth rate | 21, [0-30] | Methods |
| $\nu$ | Strength of the Allee effect | 0.01, [0.0001-1.0] | Methods |
| $k$ | Wasp interference parameter in parasitoid attack rate function | [0-30] | Methods |
| $u$ | Wasp search efficiency in parasitoid attack rate function | [0-1.0] | Methods |
| $\psi$ | Asymmetry in larval competition | 5.0, [0-100] | Methods |

**Interaction with Parasitoid Wasps:** Previous theoretical models have shown that parasitism can result in single-generation cycles (Knell 1998). We base our parasitoid model on the life-history of the common solitary endoparasitoid *A. reticulata*. As outlined in the Model System section, the wasp stage durations were assumed to be the same as those of *A. honmai*. One adult wasp of *A. reticulata* is produced per parasitized host. We assumed that the parasitized larvae and pupae have the same duration of their stages and also experience the same mortality as unparasitized ones. We define the foraging function of the female wasp as $\rho_W(\phi) = k \ln\left(1 - \frac{uW(\phi)}{k}\right) m(\phi)$, which assumes a negative binomial encounter rate that scales with temperature. The key parameters are $k$ and $u$, which are the effect of wasp interference and search efficiency respectively (Godfray & Hassell 1987; Bonsall & Eber 2001). Since we do not have any data to parameterize $k$ and $u$, we consider the range explored by Bonsall & Eber, which is $u = 0$ to $u = 1$ and $k = 0$ to $k = 30$.

**Winter Mortality:** The above five mechanisms assume that all life-history rates (i.e., birth, development and death) respond in a proportional manner to temperature. However, field researchers have hypothesized that the strong single-generation cycles in the tortrix tea pest could be the result of asymmetrical winter survival among stages in that only larvae appear to survive the winter (Furuno 1972; Kuroki & Izumi 1984). Such asymmetric winter survival is known to synchronize age-structure in a number of theoretical models of univoltine (one year for each generation) or semivoltine (multiple years for each generation) insects (Crowley et al. 1987; Gurney, Crowley, et al. 1992; Powell & Logan 2005). Therefore we evaluate the influence of differential winter survivorship on the system dynamics under a realistic temperature regime. Any functional form of mortality that increases with decreasing temperature will work for our purpose, so long as it kills a substantial number of individuals in the non-larval stages over the winter. We define the additional winter mortality rate as $n_{q_1} \exp(-n_{q_2} m(\phi))$, where $n_{q_1}$ is the maximum additional winter mortality rate, and $n_{q_2}$ controls the decrease in the additional mortality with increasing

**Table 3.** Model parameters

| Model | SLDD† | ALDD† | Sen. | Allee | Para.† | W.Mort. | GCP |
|---|---|---|---|---|---|---|---|
| Model A | √ | | | | | | 31–40 |
| Model B | √ | | √ | | | | 32 |
| Model C | √ | | | √ | | | 50 |
| Model D | √ | | | | √ | | 240 |
| Model E | | √ | | | | | 14 |
| Model F | | √ | √ | | | | 14 |
| Model G | | √ | | √ | | | 14 |
| Model H | | √ | | | √ | | 240 |
| Model I | | | | | √ | | 240 |
| Model J | √ | | | | | √ | 40 |
| Model K | √ | | √ | | | √ | 32 |
| Model L | √ | | | √ | | √ | 40 |

SLDD: symmetric larval density dependence; ALDD: asymmetrical larval density dependence; Sen: adult senescence; Allee: mate-finding limitation; Para: parasitoid interaction; W.Mort.: winter mortality; GCP: generational cycle period. † density-dependent mechanisms.

temperature. Combining the winter mortality with background mortality yields a stage-specific mortality rate of $\delta_i(\phi) = (n_i + n_{q_1}\frac{\exp(-n_{q_2}m(\phi))}{m(\phi)})m(\phi)$. Since we do not have any data to estimate $n_{q_1}$ and $n_{q_2}$, we arbitrarily define them so that winter temperatures kill a sufficient proportion of the non-larval stages in winter (mean total survival rates from December to February were set at $3.0 \times 10^{-19}$, $3.8 \times 10^{-19}$ and $2.7 \times 10^{-19}$ for egg, pupa and adult cohorts respectively), but does not affect the survival rate from March to November. The new mortality function does not scale proportionally with the physiological scale transformation, and the phi-scale equations retain periodic temperature-dependent terms (i.e., $m(\phi)$). Thus, to simulate dynamics with this level of biological mechanism, it is necessary to force the system with an explicit seasonal temperature driver. We use the smoothed daily mean temperature from meteorological records from the Chiran township. Smoothing was done conducted with a cubic smoothing spline ($df = 1000$).

# RESULTS

## Periodogram of Tortrix Moth Dynamics

Wavelet analysis of 48 years of data revealed that there were two major cycle frequencies in the *A. honmai* system. One is observed around a period of $\phi = 160$, which correspond to an annual cycle on the physiological time scale ($\phi = 161.6$) calculated directly from the temperature record (Figure 2). The other and more dominant one is located at $\phi = 32.5$, which is a little longer, but nearly concordant with, the physiological time required for egg to adult senescence ($\phi = 30.8$) estimated from laboratory data (see Appendix A). Both the annual and single-generation cycles were highly significant using a randomization test (Figure 2). Note that the third intermediate period (around $\phi = 75$) is much less important but still significant. In the following sections, we compare the predicted periodicity from the six mechanisms with this wavelet analysis to assess the extent to which a laboratory based life-cycle, and idealized forms of larval density-dependence, winter mortality and parasitism can explain the observed dynamics.

## Models without Additional Winter Mortality

Each of the biological mechanisms was able to generate cycles over some range of the parameter space explored (Figure 3, Figure 4, Table 3, and Appendix C). Symmetric larval density-dependence (Model A; Figure 3) generates cycles when both the birth rate and adult mortality are high. While it changes across mortality, the cycles occur at a period between $\phi = 31$ to $\phi = 40$, which at the lower end is similar to the period of the generation cycle observed in the empirical data. The shorter period cycle is found under high birth rate ($c$) and a high adult mortality rate ($n_A$). Asymmetrical larval density-dependence (Model E; Figure 3b) generates cycles with a shorter period at $\phi = 14$ than found under symmetric larval density-dependence. In the presence of symmetric larval density-dependence, senescence (Model B; Figure 3c) generated cycles over a wide range of birth rates with a consistent period of $\phi = 32$, which is concordant with the empirical data. Overall, the birth rate $c$ had the greatest influence on the strength of competition by impacting larval density, while the intensity of larval density-dependence ($n_C$) did not affect the dynamics.

Allee effects, again in the presence of symmetric larval density-dependence (Model C; Figure 3d), generated cycles only over a very small range of parameters, and with a period that is longer than from larval density-dependence in isolation at $\phi = 50$. The addition of parasitoids had a strong impact on the tendency for the system to cycle (Model I; Figure 3e), but with a very long (multi-generational) period around $\phi = 240$.

When in combination, the different mechanisms produced similar results as when in isolation, but with some of the mechanisms having a more dominant influence on the dynamics ( Table 3). Parasitism always generated slow cycles with a period of $\phi = 240$, regardless of the other mechanisms present. In the absence of parasitism, asymmetrical larval competition always generated fast cycles with a period of $\phi = 14$ when the degree of asymmetry ($\psi$) is strong; otherwise it had a stabilizing effect. The dynamics under symmetric larval competition changed depending on the mechanism it was paired with. Symmetric competition in isolation generated cycles with a period from $\phi = 31$ to $\phi = 40$. In the presence of an Allee effect, the period was $\phi = 50$, and the combination of symmetrical larval competition and adult senescence generated cycles with a period of $\phi = 32$, which is similar to the period found in the empirical data.

## Models with Additional Winter Mortality

While the birth, development and mortality functions are strongly temperature-dependent, they have a proportional dependence that makes them cancel out on the physiological scale. As a result, the stability and amplitude of the cycles observed on the physiological scale hold true for *all* temperature dynamics. Differential winter mortality, however, does not have this property of proportional temperature dependence so the dynamics even on the physiological scale depend on the exact patterns of fluctuations in temperature (rather than just the total annual degree days). Under the local temperature regime, the models with symmetric larval density-dependence generated frequency spectra with the two dominant peaks, which is very similar to what was observed in data (Figure 4). The primary distinction among the three

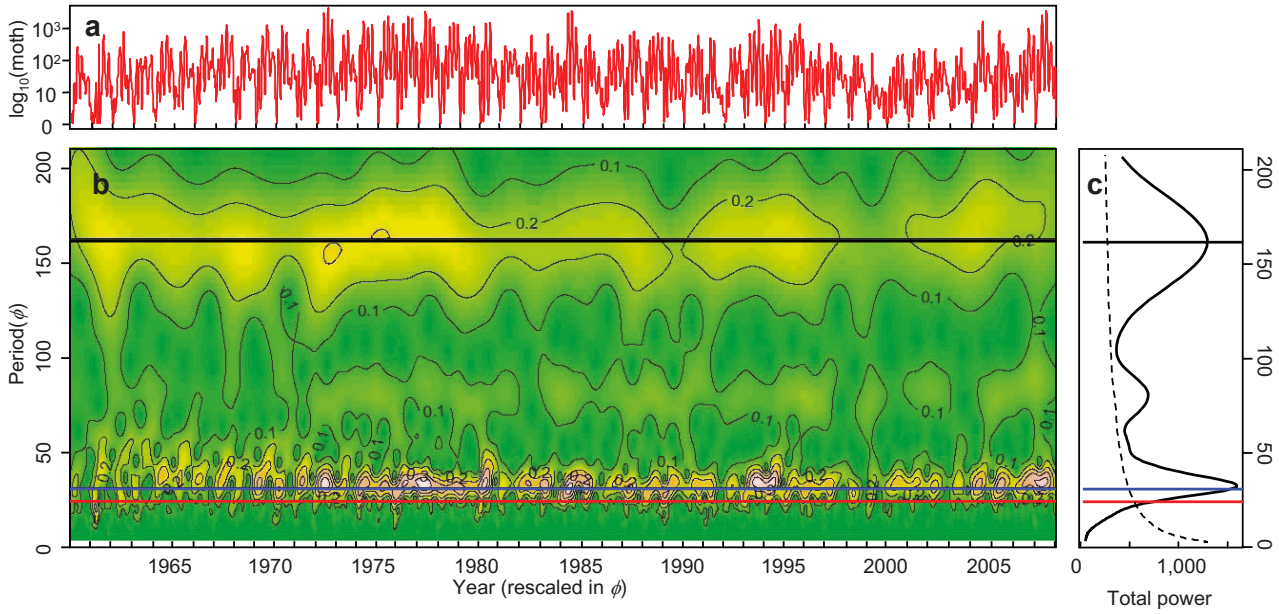


**Figure 2.** Wavelet analysis of moth dynamics. **a**, Smoothed dynamics of moth counts on the physiological scale, $\phi$. **b**, Wavelet analysis, using the Morlet wavelet with eight octaves and 16 scales. **c**, Global spectrum of the dynamics across the sum of the local wavelets across years. The dashed line shows the 99% confidence limits of the global spectrum based on 1,000 bootstrap resamples of the original data. Horizontal lines denote the physiological time units required from egg to adult (red line, $\phi = 24.1$), from egg to adult senescence (blueline, $\phi = 30.8$), and for the annual cycle (black line, $\phi = 161.6$).

model variants is in the period of the generation cycle, which is $\phi = 40$ for asymmetrical larval density-dependence either with (Model L) or without (Model J) an Allee effect, and is $\phi = 32$ for symmetric larval density-dependence with senescence (Model K). Moreover, Model K has even a close match to the small but significant third intermediate peak in the power spectrum at $\phi = 75$.

Differences among the models can also be seen in the overall character of the dynamics. In Model L and Model J, the predicted moth abundance fluctuated a little at the beginning of each year, but soon converged to the fixed point and crashed at the end of each year (Figure 4a, Figure 4c). On the other hand, the population dynamics of the model variant with adult senescence (Model K) produce sustained cycles throughout the year with a striking similarity to that of the field data (Figure 4b). To quantify the agreement between these model variants and the field data, we calculate the proportion of variation explained by each model variant. The coefficient of determination for symmetric larval density-dependence with or without Allee effects was $R^2 = 0.18$, whereas the coefficient of determination for symmetric larval density-dependence with senescence was the highest at $R^2 = 0.32$. Therefore, we conclude that the field data support the effect of adult senescence on its sustainable cycles.

## DISCUSSION

The smaller tea tortrix (*A. honmai*) in Japan exhibits 4-5 regular outbreaks a year resulting from strong generation separation and violent single-generation cycles. Many field researchers had presumed that it is the natural consequence of the seasonality (Furuno 1972; Kuroki & Izumi 1984). Only larvae survive to the end of the winter resulting in a synchronized cohort restarting spring growth. The generation cycles observed even after the second generation might have been merely a transient dampened oscillation (Taylor 1979). However our series of models revealed that the combination of symmetric larval density-dependence and rapid adult senescence is the most plausible explanation and predicts the strong and persistent generation cycles. The models without this set of mechanisms cycles of the wrong length or only rapidly dampening transients. Though previous mathematical models for laboratory (Briggs et al. 2000; Gurney, Nisbet & Lawton 1983; Gurney & Nisbet 1985; Nisbet & Onyiah 1994; Nakamura et al. 2004) or free-living (Godfray & Hassell 1987; Godfray & Hassell 1989) populations, have shown that several different mechanisms can create generation cycles neither asymmetrical competition among stages or host-parasitoid interactions can account for the behaviour when considering the detailed life-histories of the moth and its natural enemies.

Qualitatively speaking, our conclusion is in broad agreement with the conclusion of Gurney & Nisbet (1985). They predicted that self-organsized single-generation cycles in structured models are rapidly established when instantaneous competition is combined with high adult fecundity and short reproductive duration. In our model, removal of adult senescence had a stabilizing effect on the system and the population shows a brief damped oscillation with convergence on a fixed point (Appendix C). Though certain parameter combinations still permitted persistent cycles, they were typically with a period that was too long (Table 3). Gurney & Nisbet (1985) similarly showed that prolonged reproductive lifespan stabilizes dynamics. Generally speaking a short reproductive lifespan can be achieved either by scenesence (which result in a truncated age-distribution of reproducing adults) or severe

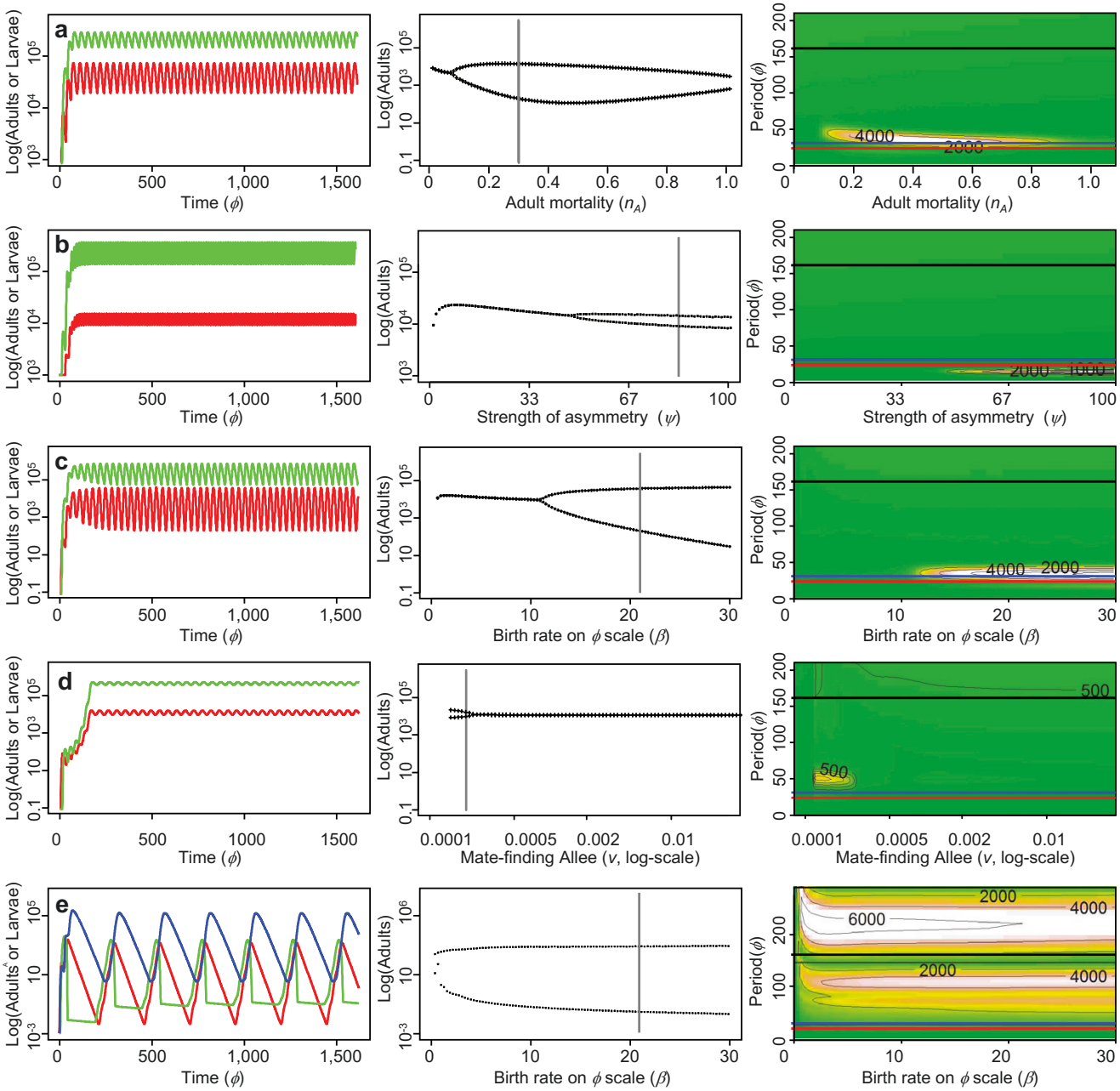


**Figure 3.** Illustrative model dynamics for each mechanism. The left-hand panel shows adult (red) and larval (green) dynamics; in the middle panel is the bifurcation plot showing the maximum and minimum of adult abundance as a function of a model parameter; and the right-hand panel shows a color map of the corresponding periodogram. The vertical gray line in the middle panel indicates parameter location for the simulation in the left-hand panel. Horizontal lines on the periodogram are the reference lines from figure 2. **a**, Symmetric larval competition (model A); **b**, asymmetric larval competition (model E); **c**, adult senescence (model B); **d**, mate-finding Allee effect (model C); **e**, interaction with parasitoid wasps (model I); the blue line in the left-hand panel represents adult-wasp dynamics. Parameters are as in Table 2, with the exception of $c = 40$ for model A (**a**), $\psi = 80$ for model E (**b**), and $\nu = 0.002$ for model C (**d**).

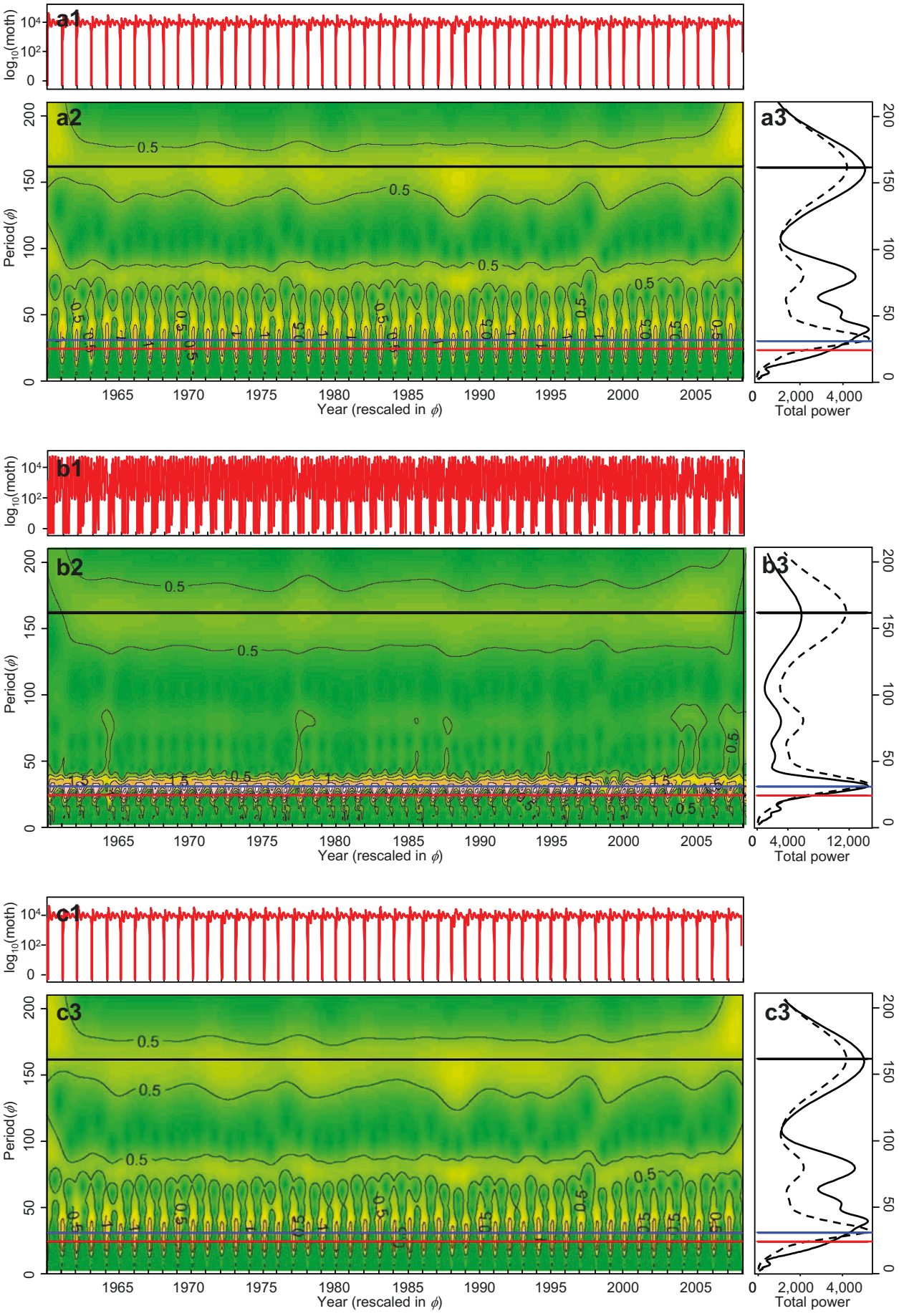


**Figure 4.** Simulated dynamics of three models under realistic temperature regime. **a**, Symmetric larval competition without adult senescence (model J). **b**, Symmetric larval competition with adult senescence (model K). **c**, Symmetric larval competition with an Allee effect (model L). See Figure 2 for panel descriptions

adult mortality (which results in a steeply declining exponential age-distribution). When investigating this difference in modeling mortality, we found that both adult senescence and a severe adult mortality can create generation cycles. Since the laboratory data support the existence of adult senescence, and adult mortality would certainly need to be much higher in nature than seen in the laboratory to generate cycles with the correct frequency, we conclude that adult senescence is a parsimonious ingredient.

The three other broad mechanisms that have been invoked to explain single-generation cycles in insects (asymmetric competition, mate-finding Allee effects and host-parasitoid interactions) do not appear to be causing cycles in the tortrix system. Asymmetric larval competition, with or without adult senescence (Model E and F), showed either no cycles with the most plausible parameters, or cycles that were much too fast (near half the generation length). Similar conclusions were reached by Briggs et al. (2000) in their model of the generation cycle in the Indian meal moth (*Plodia interpuntella*). In that case, additional egg cannibalism was required to generate the generation cycle. The smaller tea tortrix is a strict herbivore for which cannibalism has never been reported. Srinivasa & Muralimohan (2008) suggested mate-finding Allee effects as an alternative mechanism for generating single-generation cycles. Our models show that this is an unlikely cause in our system; a weak mate-finding Allee effect did generally not change the system behavior in the model variants. When the Allee effect is severe (for which there is no biological evidence), a cycle appears with a period of $\phi = 50$ which is much slower than we observed in nature ($\phi = 32.5$).

Finally, all model variants involving interactions with parasitoids exhibited a slow multigenerational cycle (around $\phi = 240$) that would take longer than a year to complete. Murdoch et al. (2002) established that consumer-resource interactions often generates multigenerational cycles with a period 4-6 times the generation length. Although, parasitoids are known to generate sustained generation cycles if the parasitoid generation time is different from that of the host (e.g. 0.5 or 1.5 length of the host) (Godfray & Hassell 1989; Godfray & Hassell 1987; Knell 1998; Bjørnstad, Sait, et al. 2001). The two dominant parasitoid wasps of *A. honmai*, *A. reticulata* and *A. adoxophyesi*, have life cycles that are synchronized and of similar length to the host (Takagi 1974; Yukinari 1976; Nakai 2009). There is no major wasp with a shorter generation time than its host in the tea pest system. Consequently, none of the models involving parasitoids can account for the observed cycles.

Anthropogenic interventions such as plucking of tea leaf and pesticide applications may provide an alternative explanation for the cycle. As the light trap census had been utilized to decide the timing of pesticide applications, it is conceivable that strictly periodic management could induce apparent cycles. However, *A. honmai* is capable of flying more than 5 km per night (Shirai & Kosugi 2000) and there are many tea orchards with different management schedules around our station. So while we cannot eliminate the possibility of a human effect, the hypothesis of a seasonally forced life-history with larval competition and adult senescence is a parsimonious explanation.

In this study, we explored a series of plausible mechanisms that could account for a sustained generation cycle observed in a multi-voltine pest insect in a temperate zone. We combine time series analysis with a mechanistic modeling approach using a suite of delayed differential equations defined on a physiological time-scale to incorporate realistic temperature dependence. We show that the most parsimonious explanation for the observed dynamics is a surprisingly simple seasonally-forced model involving larval competition and rapid adult senescence. Interactions with parasitoid wasps (Godfray & Hassell 1989) and/or asymmetrical larval density-dependence (Briggs et al. 2000) that can account for single-generation cycles in other systems, predicts cycles with the wrong period in this tortix tea pest system. We believe our general approach is applicable to a wide range of organisms with temperature-dependent life-histories, and may prove particularly useful in temperate systems where insect pest outbreaks are both density- and temperature-dependent.

## ACKNOWLEDGEMENTS

Our work greatly owes to the tireless efforts of all those entomologists in Kagoshima Prefecture who recorded light-trap catches over nearly a half-century. We thank S. Urano, the representative of PECO-IPM PILOT, Japan, who connected the studies of field and theoretical entomologists in this article, and C. Cressler for valuable comments on the manuscript. W.A.N. was supported by Natural Sciences and Engineering Research Council Discovery grants. O.N.B. received support from the U.S. Department of Agriculture's National Research Initiative.

### Data Accessibility

The data supporting this study are not publicly available.

### Competing Interests

The authors declare no conflict of interest.

## REFERENCES

Andrewartha HG & Birch LC (1954). *The distribution and abundance of animals*. Chicago: 782. URL: https://archive.org/details/distributionabun0000andr.

Baltensweiler W (1993). Why the larch bud-moth cycle collapsed in the subalpine larch-cembran pine forests in the year 1990 for the first time since 1850. *Oecologia* 94: 62–66. DOI: 10.1007/bf00317302.

Baskerville GL & Emin P (1969). Rapid estimation of heat accumulation from maximum and minimum temperatures. *Ecology* 50: 514–517. DOI: 10.2307/1933912.

Berryman AA (2002). *Population cycles: the case of trophic interactions*. Oxford. URL: https://books.google.co.jp/books?id=TClnDAAAQBAJ.

Bjørnstad ON & Grenfell BT (2001). Noisy clockwork: Time series analysis of population fluctuations in animals. *Science* 293: 638–643. DOI: 10.1126/science.1062226.

Bjørnstad ON, Sait SM, Stenseth NC, Thompson DJ & Begon M (2001). The impact of specialized enemies on the dimensionality of host dynamics. *Nature* 409: 1001–1006. DOI: 10.1038/35059003.

Bonsall MB & Eber S (2001). The role of age-structure on the persistence and the dynamics of insect herbivore-

parasitoid interactions. *Oikos* 93: 59–68. DOI: 10.1034/j.1600-0706.2001.930106.x.

Briggs CJ, Sait SM, Begon M, Thompson DJ & Godfray HCJ (2000). What causes generation cycles in populations of stored-product moths? *Journal of Animal Ecology* 69: 352–366. DOI: 10.1046/j.1365-2656.2000.00398.x.

Carmona R, Hwang W.-L & Torrésani B (1998). *Practical time-frequency analysis: Gabor and wavelet transforms with an implementation in S*. Wavelet Analysis and Its Applications. San Diego: Academic Press. ISBN: 0-12-160170-6. URL: https://books.google.co.jp/books?id=npKidakyMsC.

Costantino RF, Desharnais RA, Cushing JM & Dennis B (1997). Chaotic dynamics in an insect population. *Science* 275: 389–391. DOI: 10.1126/science.275.5298.389.

Crowley PH, Nisbet RM, Gurney WSC & Lawton JH (1987). Population regulation in animals with complex life-histories: formulation and analysis of a damselfly model. *Advances in Ecological Research* 17: 1–59. DOI: 10.1016/s0065-2504(08)60243-3.

Dennis B (1989). Allee effects: Population growth, critical density, and the chance of extinction. *Natural Resource Modeling* 3: 481–538. DOI: 10.1111/j.1939-7445.1989.tb00119.x.

Ellner SP, Bailey BA, Bobashev GV, Gallant AR, Grenfell BT & Nychka DW (1998). Noise and nonlinearity in measles epidemics: Combining mechanistic and statistical approaches to population modeling. *The American Naturalist* 151: 425–440. DOI: 10.2307/2463521.

Elton CS (1924). Periodic fluctuations in the numbers of animals: Their causes and effects. *Journal of Experimental Biology* 2: 119–163. DOI: 10.1242/jeb.2.1.119.

Furuno T (1972). Studies on the seasonal prevalence of the tea insect pests using light trap for forecasting. *Bulletin of Miyazaki Agricultural Experiment Station* 7: 1–6.

Godfray HCJ & Hassell MP (1987). Natural enemies may be a cause of discrete generations in tropical insects. *Nature* 327: 144–147. DOI: 10.1038/327144a0.

— (1989). Discrete and continuous insect populations in tropical environments. *Journal of Animal Ecology* 58: 153–174. DOI: 10.2307/4992.

Grenfell BT, Bjørnstad ON & Kappey J (2001). Travelling waves and spatial hierarchies in measles epidemics. *Nature* 414: 716–723. DOI: 10.1038/414716a.

Gurney WSC, Blythe SP & Nisbet RM (1980). Nicholson blowflies revisited. *Nature* 287: 17–21. DOI: 10.1038/287017a0.

Gurney WSC, Crowley PH & Nisbet RM (1992). Locking life-cycles onto seasons - Circle-map models of population-dynamics and local adaptation. *Journal of Mathematical Biology* 30: 251–279. DOI: 10.1007/bf00176151.

Gurney WSC & Nisbet RM (1998). *Ecological dynamics*. New York: Oxford University Press.

Gurney WSC, Nisbet RM & Lawton JH (1983). The systematic formulation of tractable single-species population-models incorporating age structure. *Journal of Animal Ecology* 52: 479–495. DOI: 10.2307/4567.

Gurney WSC & Nisbet RM (1985). Fluctuation periodicity, generation separation, and the expression of larval competition. *Theoretical Population Biology* 28: 150–180. DOI: 10.1016/0040-5809(85)90026-7.

Kainoh Y & Tamaki Y (1982). Searching behavior and oviposition of the egg-larval parasitoid, Ascogaster reticulatus WATANABE (Hymenoptera: Braconidae). *Applied Entomology and Zoology* 17: 194–206. DOI: 10.1303/aez.17.194.

Keitt TH & Urban DL (2005). Scale-specific inference using wavelets. *Ecology* 86: 2497–2504. DOI: 10.1890/04-1016.

Kendall BE, Ellner SP, McCauley E, Wood SN, Briggs CJ, Murdoch WW & Turchin P (2005). Population cycles in the pine looper moth: Dynamical tests of mechanistic hypotheses. *Ecological Monographs* 75: 259–276. DOI: 10.1890/03-4056.

Knell RJ (1998). Generation cycles. *Trends in Ecology Evolution* 13: 186–190. DOI: 10.1016/S0169-5347(97)01321-9.

Kodomari S, Tatara A, Kosugi Y & Nishijima T (2003). *Visual guide of the tea pests and pathogens: new series*. Shizuoka: Chamber of Tea Association of Shizuoka Prefecture.

Kuroki K & Izumi K (1984). A consideration on the forecasting of occurrence of the smaller tea tortirx, Adoxophyes sp. Japanese. *Bulletin of the Yamaguchi Agricultural Experiment Station* 36: 61–65. URL: https://agriknowledge.affrc.go.jp/RN/2010300486.pdf.

McCauley E, Nelson WA & Nisbet RM (2008). Small-amplitude cycles emerge from stagestructured interactions in Daphnia - algal systems. *Nature* 455: 1240–1243. DOI: 10.1038/nature07220.

Murdoch WW, Kendall BE, Nisbet RM, Briggs CJ, McCauley E & Bolser R (2002). Single-species models for many-species food webs. *Nature* 417: 541–543. DOI: 10.1038/417541a.

Nabeta FH, Nakai M & Kunimi Y (2005). Effects of temperature and photoperiod on the development and reproduction of Adoxophyes honmai (Lepidoptera: Tortricidae). *Applied Entomology and Zoology* 40: 231–238. DOI: 10.1303/aez.2005.231.

Nakai M (2009). Biological control of Tortricidae in tea fields in Japan using insect viruses and parasitoids. *Virologica Sinica* 24: 323–332. DOI: 10.1007/s12250-009-3057-9.

Nakamura K, Hasan N, Abbas L, Godfray HCJ & Bonsall MB (2004). Generation cycles in Indonesian lady beetle populations may occur as a result of cannibalism. *Proceedings of the Royal Society of London Series B-Biological Sciences* 271: S501–S504. DOI: 10.1098/rsbl.2004.0231.

Nicholson AJ (1954a). An outline of the dynamics of animal populations. *Australian Journal of Zoology* 2: 9–65. DOI: 10.1071/zo9540009.

— (1954b). Compensatory reactions of populations to stress, and their evolutionary significance. *Australian Journal of Zoology* 2: 1–8. DOI: 10.1071/zo9540001.

Nisbet RM (1996). "Delay-differential equations for structured populations". *Structured-population models in marine, terrestrial, and freshwater systems*. Ed. by S Tuljapurkar & H Caswell. Florence: International Thomson Publishing: 89–118. URL: https://books.google.co.jp/books?id=3PXi3ERgxggC.

Nisbet RM & Gurney WSC (1983). The systematic formulation of population-models for insects with dynamically varying instar duration. *Theoretical Population Biology* 23: 114–135. DOI: 10.1016/0040-5809(83)90008-4.

Nisbet RM & Onyiah LC (1994). Population dynamic consequences of competition within and between age classes.

*Journal of Mathematical Biology* 32: 329–344. DOI: 10.1007/bf00160164.

Powell JA & Logan JA (2005). Insect seasonality: circle map analysis of temperature-driven life cycles. *Theoretical Population Biology* 67: 161–179. DOI: 10.1016/j.tpb.2004.10.001.

R Development Core Team (2011). *R: A language and environment for statistical computing. R Foundation for statistical computing*. URL: https://www.r-project.org/.

Roltsch WJ, Zalom FG, Strawn AJ, Strand JF & Pitcairn MJ (1999). Evaluation of several degree-day estimation methods in California climates. *International Journal of Biometeorology* 42: 169–176. DOI: 10.1007/s004840050101.

Royama T, MacKinnon WE, Kettela EG, Carter NE & Hartling LK (2005). Analysis of spruce budworm outbreak cycles in New Brunswick, Canada, since 1952. *Ecology* 86: 1212–1224. DOI: 10.1890/03-4077.

Shimada M & Tuda M (1996). Delayed density dependence and oscillatory population dynamics in overlapping-generation systems of a seed beetle Callosobruchus chinensis: Matrix population model. *Oecologia* 105: 116–125. DOI: 10.1007/bf00328799.

Shirai Y & Kosugi Y (2000). Flight activity of the smaller tea tortrix, Adoxophyes honmai (Lepidoptera: Tortricidae). *Applied Entomology and Zoology* 35: 459–466. DOI: 10.1303/aez.2000.459.

Srinivasa YB & Muralimohan K (2008). Current theories may be inadequate to elucidate discrete generation cycles in aseasonal insects. *Current Science* 94: 1246–1249. URL: https://www.jstor.org/stable/24100229.

Takagi K (1974). Monitoring of hymenopterous parasites in tea field. Japanese. *Bulletin of the National Research Institute for Tea* 10: 91–131. URL: https://agriknowledge.affrc.go.jp/RN/2010821342.pdf.

Tamaki Y (1991). "Tortricid in tea". *Tortricid pests: their biology, natural enemies, and control*. Ed. by LPS van der Geest & HH Evenhuis. Amsterdam: Elsevier: 541–551. URL: https://shop.elsevier.com/books/tortricid-pests/van-der-geest/978-0-444-88000-0.

Taylor F (1979). Convergence to the stable age distribution in populations of insects. *The American Naturalist* 113: 511–530. DOI: 10.1086/283410.

Torrence C & Compo GP (1998). A practical guide to wavelet analysis. *Bulletin of the American Meteorological Society* 79: 61–78. DOI: 10.1175/1520-0477(1998)079%3C0061:apgtwa%3E2.0.co;2.

Yamanaka T & Liebhold AM (2009). Mate-location failure, the Allee effect and the establishment of invading populations. *Population Ecology* 51: 337–340. DOI: 10.1007/s10144-009-0158-0.

Yamanaka T, Tatsuki S & Shimada M (2008). Adaptation to the new land or effect of global warming? - An age-structured model for rapid voltinism change in an alien lepidopteran pest. *Journal of Animal Ecology* 77: 585–596. DOI: 10.1111/j.1365-2656.2008.01367.x.

Yukinari M (1976). Parasites attacking the larvae of Adoxophyes orana FISCHER VON ROSLERSTAMM amd A. fasciata WALSINGHAM in Tokushima. Japanese with English summary. *Japanese Journal of Applied Entomology and Zoology* 20: 15–20. DOI: 10.1303/jjaez.20.15.

Top, extended tea orchards in Kagoshima prefecture. The smaller tea tortrix moth (*Adoxophyes honmai*) is one of the serious pests in tea orchards all over Japan. Bottom, a larva (left) and a female moth (right). Photographs by Hiroshi Suenaga.

# Supporting Information:

# Generation separation in simple structured life-cycles: models and 48 years of field data on a tea tortrix moth

Takehiko Yamanaka, William A. Nelson, Koichiro Uchimura, Ottar N. Bjørnstad



This is the accepted version of the following article: Yamanaka T. et al. (2012) *The American Naturalist* 179: 95-109.
The final published version is available at: https://doi.org/10.1086/663201.

## Appendix A: Temperature-Dependent Birth, Death, and Development Rate Functions

As with most insects, the birth rate, stage-specific death rates and stage-specific development rates of *A. honmai* are strongly temperature-dependent. We parameterize this temperature dependence using data from laboratory experiments by Nabeta et al. (2005), and from data using insects in the Miyazaki Prefecture (Kodomari et al. 2003). Data include observations of birth rate, development time for eggs, larvae and pupae, as well as survivorship for all stages at a range of temperatures. The pattern of adult survivorship (see Nabeta et al. 2005) suggests that adults divide into two sub-stages based on age. The first contains young adults who suffer a relatively low mortality, and the second contains older adults who have much higher mortality rates. The age of transition between the two sub-stages is temperature dependent, and correlates closely to the cessation of reproduction. Thus, we subdivide the adult stage into reproductive and senescent stages. Since only non-senescent adults reproduce, and the senescent mortality rate is much higher than the non-senescent rate, we only include reproductive adults in the model (Table 1). The reproductive stage duration was calculated as the time to 50% survival.

Development rates increase with increasing temperature in all stages (Figure A1). The empirical data suggest a development rate function ($h_i(t)$) of the logistic form

$$h_i(t) = \frac{\alpha_i}{1 + \exp\left(-\gamma_D(D(t) - h_D)\right)} \tag{A1}$$

where $D(t)$ is the temperature (degrees Celsius) at time $t$, $h_D$ is the temperature at which the development rate function reaches half the asymptotic value, $\alpha_i$ is a scaling coefficient, and $\gamma_D$ controls the steepness of the logistic function. We first estimate the parameters $\alpha$, $h_D$ and $\gamma_D$, which are common to all stages, by fitting eq. $(A1)$ to total duration from egg to pupa using a minimum least-squares objective. Using the common $h_D$ and $\gamma_D$, the $\alpha_i$ for each stage was estimated in eq. $(A1)$ is subsequently estimated by fitting the stage-specific development rates using the same minimum least-squares objective. The two larval stages are split at the midpoint of the larval development period ($\alpha_L$), and both larval sizes are assumed to have the same development rate, which is double that of the full larval stage to ensure that cohorts transition through the two substages at the time for the full stage (i.e., $\alpha_{L_1} = \alpha_{L_2} = 2\alpha_L$).

Stage-specific mortality data are available in the form of through-stage survivorship at each temperature. We convert these to daily mortality rates ($d_{obs}$) using the relationship, $d_{obs} = -\log(\sigma_{obs})/\tau_{obs}$, where $\sigma_{obs}$ is the observed survivorship, and $\tau_{obs}$ is the observed mean development time. Daily mortality rates generally increased with temperature (Figure A2). With the aim of simplifying the model, we fit a mortality function using the same generic base function as the development rate. Namely $d_i(t) = n_i g(t)$, where $g(t) = 1/(1 + \exp\left(-\gamma_D(D(t) - h_D)\right))$ and $n_i$ is a stage-specific scalar. The mortality data are more variable than development data, but the mortality rate function yields a reasonable fit to the data, with the exception of some mismatches in the larval and pupal stages at high temperature. Using the same base function for mortality as found for the development rates greatly simplifies analysis of the model (see below), and had little impact on the predicted population dynamics. The per capita birth rates also show an increase with higher temperature (Figure A3). Following the same rationale as for the mortality rate, we assumed a functional form that is proportional to the base function $b(t) = cg(t)$. Fit parameter values are shown in Table 2.

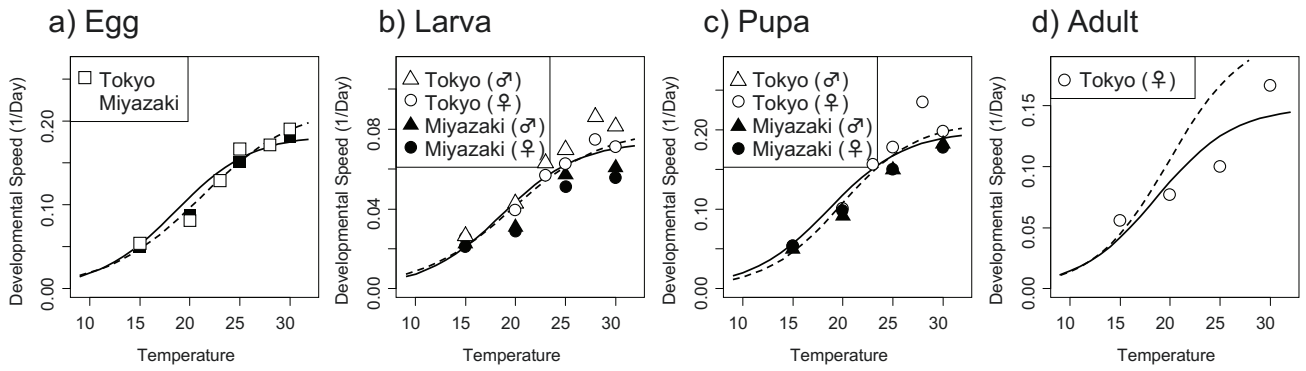


**Figure A1.** Stage-specific development rate ($h_i(t)$) of female moths as a function of temperature. Data are from Tokyo (open symbols) or from Miyazaki Prefecture (filled symbols) for **a)** Egg, **b)** Larval, **c)** Pupal, and **d)** Reproductive (non-senescent) adult stages. The development rate function is assumed to share the common scaling parameters $h_D$ and $\gamma_D$ for all stages, but the constants of proportionality $\alpha_i$ are different for each stage. The solid lines show the fit function and the dotted lines represent the alternative fit function changing not only $\alpha_i$ but also $h_D$ and $\gamma_D$. See Table 2 for fit parameter values.

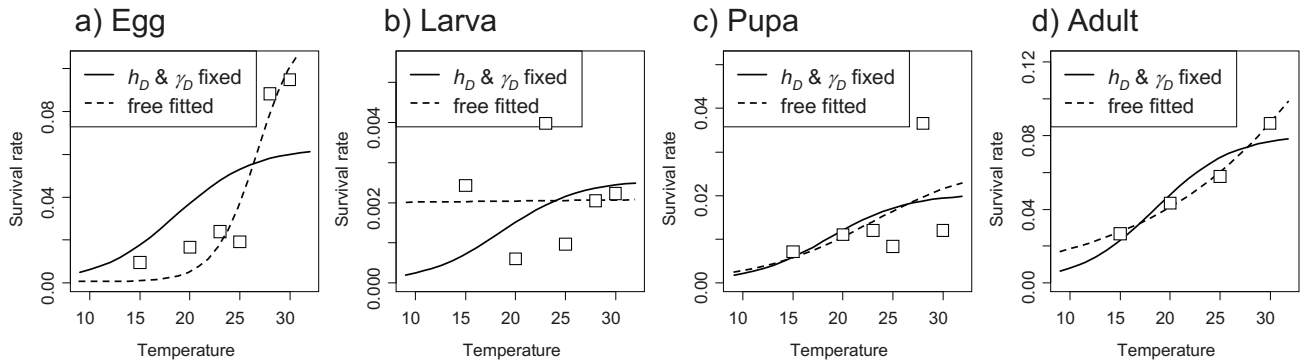


**Figure A2.** Stage-specific mortality rate ($\delta_i(t)$) of female moths as a function of temperature. Data are from Tokyo for **a)** Egg, **b)** Larval, **c)** Pupal, and **d)** Reproductive (non-senescent) adult stages. The mortality rate function is assumed to have the same base function (i.e., $g(t)$) as the developmental rate, and a constant of proportionality $n_i$ that is different for each stage. The dashed lines show the function which are fitted not only with $\delta_i$, but also $h_D$ and $\gamma_D$. The solid lines show the function with $h_D$ and $\gamma_D$ fixed at the estimates from the development rate data. See Table 2 for fit parameter values.

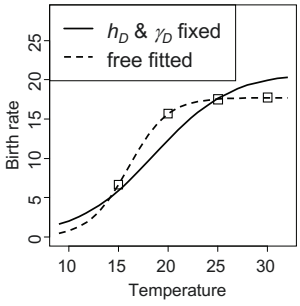


**Figure A3.** Per-capita birth rate (b(t)) as a function of temperature. Data are from Tokyo. We assume a birth rate function of the form using the base function with a constant of proportionality $c$. The dashed lines show the function which are fitted not only with $\delta_i$, but also $h_D$ and $\gamma_D$. The solid lines show the function with $h_D$ and $\gamma_D$ fixed at the estimates from the development rate data. See Table 2 for fit parameter values.

## Appendix B: Model Development and Scale Transformation

### Time-scale model

The modeling framework developed by Nisbet & Gurney (1983), provides a basis to model population dynamics of stage-structured organisms with time-varying birth, death and development rates (e.g., due to food dynamics or seasonal temperature). In this appendix, we first layout the overall architecture of the model on a Julian time-scale. Subsequently, we transform the equations to a physiologically-based scale (hereafter referred to as the phi-scale) so that the time-varying delays become fixed delays to facilitate model analysis. The general model was developed to examine the role of density-dependence (three types), parasitism, temperature, and adult senescence on population dynamics. Each variant can be arrived at as a special case of the general model.

To incorporate the role of parasitism, the general model requires a description of both moth and parasitoid populations. The tortrix moth population is broken up into five stages: eggs ($E$), young larvae ($L_1$), old larvae ($L_2$), pupae ($P$) and adults ($A$). Wasp populations are assumed to be structured into eggs, larvae, pupae and adult. However, since the egg, larvae and pupae stages follow the same development as the *A. honmai* (Yukinari 1976; Takagi 1974), it is only necessary to explicitly track the adult wasps ($W$) and parasitized *A. honmai* stages (denoted by a $W$ superscript).

In our study we consider the egg parasitoid, *A. reticulata* (Braconidae). A female wasp oviposits on an egg of the host, *A. honmai*. A larval wasp gets into its host egg and grows inside the host body. At the end of the old larval stage, it escapes from the host tissue to pupate. For the detail biology of *A. reticulata* (Braconidae) see Kainoh & Tamaki (1982).

The model architecture is

$$\begin{aligned}
\frac{dE(t)}{dt} &= R_b(t) - R_E(t) - (d_E(t) + p_W(t))\,E(t) \\
\frac{dL_1(t)}{dt} &= R_E(t) - R_{L_1}(t) - d_{L_1}(t)L_1(t) \\
\frac{dL_2(t)}{dt} &= R_{L_1}(t) - R_{L_2}(t) - d_{L_2}(t)L_2(t) \\
\frac{dP(t)}{dt} &= R_{L_2}(t) - R_P(t) - d_P(t)P(t) \\
\frac{dA(t)}{dt} &= R_P(t) - R_A(t) - d_A(t)A(t)
\end{aligned} \tag{B1}$$

$$\begin{aligned}
\frac{dL_1^W(t)}{dt} &= p_W(t)E(t) - R_{L_1^W}(t) - d_{L_1^W}(t)L_1^W(t) \\
\frac{dL_2^W(t)}{dt} &= R_{L_1^W}(t) - R_{L_2^W}(t) - d_{L_2^W}(t)L_2^W(t) \\
\frac{dP^W(t)}{dt} &= R_{L_2^W}(t) - R_{P^W}(t) - d_{P^W}(t)P^W(t) \\
\frac{dW(t)}{dt} &= R_{P^W}(t) - d_W(t)W(t)
\end{aligned}$$

where $t$ signifies time varying functions or states on a Julian day scale, $d_i(t)$ is the per-capita mortality rate for stage $i$, and $R_i(t)$ is the recruitment out of stage $i$, where $i$ can be the unparasitized moths ($i \in E, L_1, L_2, P, A$), parasitized moths ($i \in L_1^W, L_2^W, P^W$) or the adult wasps ($i \in W$). Parasitism occurs through the per capita parasitism rate $p_W(t)$, and $R_b(t)$ represents recruitment into the egg stage from adult reproduction. Note that $R_A(t)$ represents adult senescence. Since a constant sex ratio is assumed here, only the dynamics of female moths is modeled.

Following Nisbet & Gurney (1983), the recruitment rate into the egg stage is given by

$$R_b(t) = b(t)A(t) \tag{B2}$$

where $b(t)$ is the per-capita birth rate, and recruitment into all other stages is

$$R_{i+1}(t) = R_i(t - \tau_i(t))S_i(t)\frac{h_i(t)}{h_i(t - \tau_i(t))} \tag{B3}$$

where $\tau_i(t)$ is the duration of stage $i$ at time $t$, $h_i(t)$ is the development rate, and $S_i(t)$ is the through-stage survivorship. Through-stage survivorship is calculated as

$$S_i(t) = \exp\left(-\int_{t-\tau_i(t)}^{t} d_i(x)dx\right) \tag{B4}$$

and stage durations are calculated implicitly using the development rate constraint

$$1 = \int_{t-\tau_i(t)}^{t} h_i(x)dx \tag{B5}$$

Equation ($B5$) can be used (implicitly) to determine the range in time from $t - \tau_i(t)$ to $t$ required for a cohort to complete stage $i$. In numerical simulation, however, $\tau_i(t)$ is calculated by differentiating both sides for eq. ($B5$) and solving the resulting delay-differential equation (Nisbet & Gurney 1983)

$$\frac{d\tau(t)}{dt} = 1 - \frac{h_i(t)}{h_i(t - \tau_i(t))} \tag{B6}$$

The set of delay-differential equations given by eq. ($B1$) is the general form of the model on a Julian day scale. Each model variant is arrived at by specifying a set of birth $b(t)$, death $d_i(t)$ and development $h_i(t)$ rate functions, along with the corresponding parameters. Since the development rate is temperature-dependent in this system, and temperature vary through time, stage durations will vary through time as well. These time-varying delays can be determined through an integral constraint (eq. ($B6$)), but this limits the range of mathematical tools available for analysis. Following the approach of McCauley et al. (2008), we transform the model to a physiological scale that results in fixed rather than variable stage durations (except in the specific models of stage-specific winter mortality rates).

## Physiological-scale model

When the development and mortality rates for all stages are proportional to a single time-varying factor (as laboratory data generally suggests), a transformation to the cumulative development scale results in a model with fixed rather than variable delays McCauley et al. (2008). In our model, the development rate of the moth scales with temperature as

$$h_i(t) = \frac{\alpha_i}{1 + \exp\left(-\gamma_D(D(t) - h_D)\right)} \tag{B7}$$

where $D(t)$ is the temperature at time $t$ (see Appendix A for full details). The stages differ only in their scaling coefficient $\alpha_i$. Using eq. ($B7$), the expressions used to calculate the stage durations (eq. ($B5$)) can rewritten as

$$\frac{1}{\alpha_i} = \int_{t-\tau_i(t)}^{t} g(x)dx \tag{B8}$$

where $g(t) = 1/(1 + \exp(-\gamma_D(D(t) - h_D)))$. The transformation begins by defining the new physiological scale (phi-scale) as

$$\phi(t) = \int_{0}^{t} g(x)dx \tag{B9}$$

For notational clarity, we define $m(\phi) = g(t)$ as development rate on the phi-scale. From eq. ($B9$), we can write

$$\phi(t - \tau_i(t)) = \int_{0}^{t-\tau_i(t)} g(x)dx = \int_{0}^{t} g(x)dx - \int_{t-\tau_i(t)}^{t} g(x)dx = \phi(t) - \frac{1}{\alpha_i} \tag{B10}$$

which reduces the time-varying delay to a fixed delay on the transformed scale. Survivorship equations are also transformed to the phi-scale by introducing $g(x)/g(x)$

$$S_i(t) = \exp\left(-\int_{t-\tau_i(t)}^{t} d_i(x)dx\right) = \exp\left(-\int_{t-\tau_i(t)}^{t} \frac{d_i(x)}{g(x)}\left[g(x)dx\right]\right) \tag{B11}$$

From eq. ($B9$), the term in square braces is $d\phi$, which lets us write

$$S_i(\phi) = \exp\left(-\int_{\phi-\frac{1}{\alpha_i}}^{\phi} \frac{\delta_i(\xi)}{m(\xi)}d\xi\right) \tag{B12}$$

where $\delta_i(\phi) = d_i(t)$ is the per capita mortality rate function on the phi-scale. To complete the transformation, we take the derivative of eq. ($B9$) with respect to time, which yields

$$\frac{dt}{d\phi} = \frac{1}{m(\phi)} \tag{B13}$$

Defining $\beta(\phi) = b(t)$ as the birth rate function in the phi scale, eq. ($B2$) is rewritten as

$$R_b(\phi) = \beta(\phi)A(\phi) \tag{B14}$$

and the recruitment rates in eq. ($B3$) are

$$R_{i+1}(\phi) = R_i\left(\phi - \frac{1}{\alpha_i}\right) S_i(\phi) \frac{m(\phi)}{m\left(\phi - \frac{1}{\alpha_i}\right)} \tag{B15}$$

To simplify notation, we introduce cohort-based functions for the delay and survivorship

$$\phi_i = \phi - \sum_{x=E}^{i} \frac{1}{\alpha_x} \tag{B16}$$

$$S_i(\phi) = \exp\left(-\sum_{x=E}^{i} \int_{\phi_x}^{\phi_{x-1}} \frac{\delta_x(\xi)}{m(\xi)} d\xi\right), \text{ where } \phi_{E-1} \equiv \phi \tag{B17}$$

where $\phi_i$ is the fixed stage duration from the beginning of the egg stage to the end of stage $i$ ($i \in \{E, L_1, L_2, P, A\}$). $S_i(\phi)$ is through-stage survivorship from the beginning of the egg stage born at delayed physiological time ($\phi_i$) to stage $i$ at current physiological time ($\phi$). Using eq. ($B13$), and substituting the above cohort-based expressions, the transformed model equations are given by eq. (3) in the methods.

## Appendix C: Model variants

Each model variant is arrived at as a special case of the general model shown in the methods (eq. (3)). The biological mechanisms contained in each model variant (Table 3) were chosen to explore various combinations of these processes, always ensuring that models included at least one negatively density dependent mechanism. The following sections detail the simplified model obtained after substituting the functions (Table 1) that correspond to each biological mechanisms (see METHODS for details).

## Model A: Symmetric larval density-dependence

$$
\begin{aligned}
\frac{dL_1(\phi)}{d\phi} &= cA(\phi_E)S_E(\phi) - cA(\phi_{L_1})S_{L_1}(\phi) - (n_L + n_C L(\phi))\, L_1(\phi) \\
\frac{dL_2(\phi)}{d\phi} &= cA(\phi_{L_1})S_{L_1}(\phi) - cA(\phi_{L_2})S_{L_2}(\phi) - (n_L + n_C L(\phi))\, L_2(\phi) \\
\frac{dA(\phi)}{d\phi} &= cA(\phi_P)S_P(\phi) - n_A A(\phi) \\
S_{L_1}(\phi) &= \exp\left( -\sum_{i=E}^{L_1} \frac{n_i}{\alpha_i} - n_C \int_{\hat{\phi}_{L_1:L_1}}^{\phi} L(\xi)d\xi \right) \\
S_{L_2}(\phi) &= \exp\left( -\sum_{i=E}^{L_2} \frac{n_i}{\alpha_i} - n_C \int_{\hat{\phi}_{L_1:L_2}}^{\phi} L(\xi)d\xi \right) \\
S_P(\phi) &= \exp\left( -\sum_{i=E}^{P} \frac{n_i}{\alpha_i} - n_C \int_{\hat{\phi}_{L_1:P}}^{\hat{\phi}_{P:P}} L(\xi)d\xi \right)
\end{aligned}
$$

where $L(\phi) = L_1(\phi) + L_2(\phi)$. $\phi_i$ and $\hat{\phi}_{j:k}$ were defined as follows and will be used in the subsequent descriptions of model variants.

$$
\begin{aligned}
\phi_i &= \phi - \sum_{x=E}^{i} \frac{1}{\alpha_x} \\
\hat{\phi}_{j:k} &= \begin{cases} \phi - \sum_{x=j}^{k} \frac{1}{\alpha_x} & \text{if } j \le k \\ \phi & \text{if } j > k \end{cases}
\end{aligned}
$$

Figure C1 shows the predicted dynamics as a function of the birth rate scalar and adult mortality.

## Model B: Symmetric larval density-dependence with senescence

$$
\begin{aligned}
\frac{dL_1(\phi)}{d\phi} &= cA(\phi_E)S_E(\phi) - cA(\phi_{L_1})S_{L_1}(\phi) - (n_L + n_C L(\phi))\, L_1(\phi) \\
\frac{dL_2(\phi)}{d\phi} &= cA(\phi_{L_1})S_{L_1}(\phi) - cA(\phi_{L_2})S_{L_2}(\phi) - (n_L + n_C L(\phi))\, L_2(\phi) \\
\frac{dA(\phi)}{d\phi} &= cA(\phi_P)S_P(\phi) - cA(\phi_A)S_A(\phi) - n_A A(\phi) \\
S_{L_1}(\phi) &= \exp\left( -\sum_{i=E}^{L_1} \frac{n_i}{\alpha_i} - n_C \int_{\hat{\phi}_{L_1:L_1}}^{\phi} L(\xi)d\xi \right) \\
S_{L_2}(\phi) &= \exp\left( -\sum_{i=E}^{L_2} \frac{n_i}{\alpha_i} - n_C \int_{\hat{\phi}_{L_1:L_2}}^{\phi} L(\xi)d\xi \right) \\
S_P(\phi) &= \exp\left( -\sum_{i=E}^{P} \frac{n_i}{\alpha_i} - n_C \int_{\hat{\phi}_{L_1:P}}^{\hat{\phi}_{P:P}} L(\xi)d\xi \right) \\
S_A(\phi) &= \exp\left( -\sum_{i=E}^{A} \frac{n_i}{\alpha_i} - n_C \int_{\hat{\phi}_{L_1:A}}^{\hat{\phi}_{P:A}} L(\xi)d\xi \right)
\end{aligned}
$$

where $L(\phi) = L_1(\phi) + L_2(\phi)$. Figure C2 shows the predicted dynamics as a function of the birth rate scalar.

## Model C: Symmetric larval density-dependence with Allee effect

$$
\begin{aligned}
\frac{dL_1(\phi)}{d\phi} &= c\left(1-e^{\nu A(\phi_E)}\right)A(\phi_E)S_E(\phi) - c\left(1-e^{\nu A(\phi_{L_1})}\right)A(\phi_{L_1})S_{L_1}(\phi) - \left(n_L + n_C L(\phi)\right)L_1(\phi)\\
\frac{dL_2(\phi)}{d\phi} &= c\left(1-e^{\nu A(\phi_{L_1})}\right)A(\phi_{L_1})S_{L_1}(\phi) - c\left(1-e^{\nu A(\phi_{L_2})}\right)A(\phi_{L_2})S_{L_2}(\phi) - \left(n_L + n_C L(\phi)\right)L_2(\phi)\\
\frac{dA(\phi)}{d\phi} &= c\left(1-e^{\nu A(\phi_P)}\right)A(\phi_P)S_P(\phi) - n_A A(\phi)\\
S_{L_1}(\phi) &= \exp\left(-\sum_{i=E}^{L_1}\frac{n_i}{\alpha_i} - n_C\int_{\hat{\phi}_{L_1:L_1}}^{\phi} L(\xi)d\xi\right)\\
S_{L_2}(\phi) &= \exp\left(-\sum_{i=E}^{L_2}\frac{n_i}{\alpha_i} - n_C\int_{\hat{\phi}_{L_1:L_2}}^{\phi} L(\xi)d\xi\right)\\
S_P(\phi) &= \exp\left(-\sum_{i=E}^{P}\frac{n_i}{\alpha_i} - n_C\int_{\hat{\phi}_{L_1:P}}^{\hat{\phi}_{P:P}} L(\xi)d\xi\right)
\end{aligned}
$$

where $L(\phi) = L_1(\phi) + L_2(\phi)$. Figure C3 shows the predicted dynamics as a function of the birth rate scalar and strength of Allee effect.

## Model D: Symmetric larval density-dependence with parasitism

$$
\begin{aligned}
\frac{dE(\phi)}{d\phi} &= cA(\phi) - cA(\phi_E)S_E(\phi) - \left(n_E + k\ln\left(1-\frac{u}{k}W(\phi)\right)\right)E(\phi)\\
\frac{dL_1(\phi)}{d\phi} &= cA(\phi_E)S_E(\phi) - cA(\phi_{L_1})S_{L_1}(\phi) - \left(n_L + n_C L(\phi)\right)L_1(\phi)\\
\frac{dL_2(\phi)}{d\phi} &= cA(\phi_{L_1})S_{L_1}(\phi) - cA(\phi_{L_2})S_{L_2}(\phi) - \left(n_L + n_C L(\phi)\right)L_2(\phi)\\
\frac{dA(\phi)}{d\phi} &= cA(\phi_P)S_P(\phi) - n_A A(\phi)\\
\frac{dW(\phi)}{d\phi} &= k\ln\left(1-\frac{u}{k}W(\phi_P)\right)E(\phi_P)S_{PW} - n_W W(\phi)\\
S_E(\phi) &= \exp\left(-\frac{n_E}{\alpha_E} - k\int_{\hat{\phi}_{E:E}}^{\phi}\ln\left(1-\frac{u}{k}W(\phi)\right)d\xi\right)\\
S_{L_1}(\phi) &= \exp\left(-\sum_{i=E}^{L_1}\frac{n_i}{\alpha_i} - k\int_{\hat{\phi}_{E:L_1}}^{\hat{\phi}_{L_1:L_1}}\ln\left(1-\frac{u}{k}W(\phi)\right)d\xi - n_C\int_{\hat{\phi}_{L_1:L_1}}^{\phi}L(\xi)d\xi\right)\\
S_{L_2}(\phi) &= \exp\left(-\sum_{i=E}^{L_2}\frac{n_i}{\alpha_i} - k\int_{\hat{\phi}_{E:L_2}}^{\hat{\phi}_{L_1:L_2}}\ln\left(1-\frac{u}{k}W(\phi)\right)d\xi - n_C\int_{\hat{\phi}_{L_1:L_2}}^{\hat{\phi}_{L_2:L_2}}L(\xi)d\xi\right)\\
S_P(\phi) &= \exp\left(-\sum_{i=E}^{P}\frac{n_i}{\alpha_i} - k\int_{\hat{\phi}_{E:P}}^{\hat{\phi}_{L_1:P}}\ln\left(1-\frac{u}{k}W(\phi)\right)d\xi - n_C\int_{\hat{\phi}_{L_1:P}}^{\hat{\phi}_{L_2:P}}L(\xi)d\xi\right)\\
S_{PW}(\phi) &= \exp\left(-\sum_{i=L_1}^{P}\frac{n_i}{\alpha_i} - n_C\int_{\hat{\phi}_{L_1:P}}^{\hat{\phi}_{L_2:P}}L(\xi)d\xi\right)
\end{aligned}
$$

where $L(\phi) = L_1(\phi) + L_2(\phi)$. Figure C4 shows the predicted dynamics as a function of the birth rate scalar, search efficiency and interference among wasps.

## Model E: Asymmetrical larval density-dependence

$$\frac{dL_1(\phi)}{d\phi} = cA(\phi_E)S_E(\phi) - cA(\phi_{L_1})S_{L_1}(\phi) - (n_L + n_C(L_1(\phi) + \psi L_2(\phi)))\, L_1(\phi)$$
$$\frac{dL_2(\phi)}{d\phi} = cA(\phi_{L_1})S_{L_1}(\phi) - cA(\phi_{L_2})S_{L_2}(\phi) - (n_L + n_C(L_1(\phi)/\psi + L_2(\phi)))\, L_2(\phi)$$
$$\frac{dA(\phi)}{d\phi} = cA(\phi_P)S_P(\phi) - n_A A(\phi)$$
$$S_{L_1}(\phi) = \exp\left(-\sum_{i=E}^{L_1}\frac{n_i}{\alpha_i} - n_C\int_{\hat{\phi}_{L_1:L_1}}^{\phi}(L_1(\xi) + \psi L_2(\xi))d\xi\right)$$
$$S_{L_2}(\phi) = \exp\left(-\sum_{i=E}^{L_2}\frac{n_i}{\alpha_i} - n_C\int_{\hat{\phi}_{L_1:L_2}}^{\hat{\phi}_{L_2:L_2}}(L_1(\xi) + \psi L_2(\xi))d\xi - n_C\int_{\hat{\phi}_{L_2:L_2}}^{\phi}(L_1(\xi)/\psi + L_2(\xi))d\xi\right)$$
$$S_P(\phi) = \exp\left(-\sum_{i=E}^{P}\frac{n_i}{\alpha_i} - n_C\int_{\hat{\phi}_{L_1:P}}^{\hat{\phi}_{L_2:P}}(L_1(\xi) + \psi L_2(\xi))d\xi - n_C\int_{\hat{\phi}_{L_2:P}}^{\hat{\phi}_{P:P}}(L_1(\xi)/\psi + L_2(\xi))d\xi\right)$$

Figure C5 shows the predicted dynamics as a function of the birth rate scalar and strength of competition asymmetry.

## Model F: Asymmetrical larval density-dependence with senescence

$$\frac{dL_1(\phi)}{d\phi} = cA(\phi_E)S_E(\phi) - cA(\phi_{L_1})S_{L_1}(\phi) - (n_L + n_C(L_1(\phi) + \psi L_2(\phi)))\, L_1(\phi)$$
$$\frac{dL_2(\phi)}{d\phi} = cA(\phi_{L_1})S_{L_1}(\phi) - cA(\phi_{L_2})S_{L_2}(\phi) - (n_L + n_C(L_1(\phi)/\psi + L_2(\phi)))\, L_2(\phi)$$
$$\frac{dA(\phi)}{d\phi} = cA(\phi_P)S_P(\phi) - cA(\phi_A)S_A(\phi) - n_A A(\phi)$$
$$S_{L_1}(\phi) = \exp\left(-\sum_{i=E}^{L_1}\frac{n_i}{\alpha_i} - n_C\int_{\hat{\phi}_{L_1:L_1}}^{\phi}(L_1(\xi) + \psi L_2(\xi))d\xi\right)$$
$$S_{L_2}(\phi) = \exp\left(-\sum_{i=E}^{L_2}\frac{n_i}{\alpha_i} - n_C\int_{\hat{\phi}_{L_1:L_2}}^{\hat{\phi}_{L_2:L_2}}(L_1(\xi) + \psi L_2(\xi))d\xi - n_C\int_{\hat{\phi}_{L_2:L_2}}^{\phi}(L_1(\xi)/\psi + L_2(\xi))d\xi\right)$$
$$S_P(\phi) = \exp\left(-\sum_{i=E}^{P}\frac{n_i}{\alpha_i} - n_C\int_{\hat{\phi}_{L_1:P}}^{\hat{\phi}_{L_2:P}}(L_1(\xi) + \psi L_2(\xi))d\xi - n_C\int_{\hat{\phi}_{L_2:P}}^{\hat{\phi}_{P:P}}(L_1(\xi)/\psi + L_2(\xi))d\xi\right)$$
$$S_A(\phi) = \exp\left(-\sum_{i=E}^{A}\frac{n_i}{\alpha_i} - n_C\int_{\hat{\phi}_{L_1:A}}^{\hat{\phi}_{L_2:A}}(L_1(\xi) + \psi L_2(\xi))d\xi - n_C\int_{\hat{\phi}_{L_2:A}}^{\hat{\phi}_{P:A}}(L_1(\xi)/\psi + L_2(\xi))d\xi\right)$$

Figure C6 shows the predicted dynamics as a function of the birth rate scalar and strength of competition asymmetry.

## Model G: Asymmetrical larval density-dependence with Allee effect

$$
\begin{aligned}
\frac{dL_1(\phi)}{d\phi} &= c\left(1-e^{\nu A(\phi_E)}\right)A(\phi_E)S_E(\phi) - c\left(1-e^{\nu A(\phi_{L_1})}\right)A(\phi_{L_1})S_{L_1}(\phi) \\
&\quad - \left(n_L + n_C(L_1(\phi)+\psi L_2(\phi))\right)L_1(\phi) \\
\frac{dL_2(\phi)}{d\phi} &= c\left(1-e^{\nu A(\phi_{L_1})}\right)A(\phi_{L_1})S_{L_1}(\phi) - c\left(1-e^{\nu A(\phi_{L_2})}\right)A(\phi_{L_2})S_{L_2}(\phi) \\
&\quad - \left(n_L + n_C(L_1(\phi)/\psi+L_2(\phi))\right)L_2(\phi) \\
\frac{dA(\phi)}{d\phi} &= c\left(1-e^{\nu A(\phi_P)}\right)A(\phi_P)S_P(\phi) - n_A A(\phi) \\
S_{L_1}(\phi) &= \exp\left(-\sum_{i=E}^{L_1}\frac{n_i}{\alpha_i} - n_C\int_{\hat{\phi}_{L_1:L_1}}^{\phi}(L_1(\xi)+\psi L_2(\xi))d\xi\right) \\
S_{L_2}(\phi) &= \exp\left(-\sum_{i=E}^{L_2}\frac{n_i}{\alpha_i} - n_C\int_{\hat{\phi}_{L_1:L_2}}^{\hat{\phi}_{L_2:L_2}}(L_1(\xi)+\psi L_2(\xi))d\xi - n_C\int_{\hat{\phi}_{L_2:L_2}}^{\phi}(L_1(\xi)/\psi+L_2(\xi))d\xi\right) \\
S_P(\phi) &= \exp\left(-\sum_{i=E}^{P}\frac{n_i}{\alpha_i} - n_C\int_{\hat{\phi}_{L_1:P}}^{\hat{\phi}_{L_2:P}}(L_1(\xi)+\psi L_2(\xi))d\xi - n_C\int_{\hat{\phi}_{L_2:P}}^{\hat{\phi}_{P:P}}(L_1(\xi)/\psi+L_2(\xi))d\xi\right)
\end{aligned}
$$

Figure C7 shows the predicted dynamics as a function of the birth rate scalar and strength of competition asymmetry.

## Model H: Asymmetrical larval density-dependence with parasitism

$$
\begin{aligned}
\frac{dE(\phi)}{d\phi} &= cA(\phi) - cA(\phi_E)S_E(\phi) - \left(n_E + k\ln\left(1-\frac{u}{k}W(\phi)\right)\right)E(\phi) \\
\frac{dL_1(\phi)}{d\phi} &= cA(\phi_E)S_E(\phi) - cA(\phi_{L_1})S_{L_1}(\phi) - \left(n_L + n_C(L_1(\phi)+\psi L_2(\phi))\right)L_1(\phi) \\
\frac{dL_2(\phi)}{d\phi} &= cA(\phi_{L_1})S_{L_1}(\phi) - cA(\phi_{L_2})S_{L_2}(\phi) - \left(n_L + n_C(L_1(\phi)+\psi L_2(\phi))\right)L_2(\phi) \\
\frac{dA(\phi)}{d\phi} &= cA(\phi_P)S_P(\phi) - n_A A(\phi) \\
\frac{dW(\phi)}{d\phi} &= k\ln\left(1-\frac{u}{k}W(\phi_P)\right)E(\phi_P)S_P w - n_W W(\phi)
\end{aligned}
$$

$$
\begin{aligned}
S_E(\phi) &= \exp\left(-\frac{n_E}{\alpha_E} - k\int_{\hat{\phi}_{E:E}}^{\phi} \ln\left(1-\frac{u}{k}W(\phi)\right)d\xi\right)\\
S_{L_1}(\phi) &= \exp\left(-\sum_{i=E}^{L_1}\frac{n_i}{\alpha_i} - k\int_{\hat{\phi}_{E:L_1}}^{\hat{\phi}_{L_1:L_1}} \ln\left(1-\frac{u}{k}W(\phi)\right)d\xi\right.\\
&\quad \left. -n_C\int_{\hat{\phi}_{L_1:L_1}}^{\phi} L_1(\xi)+\psi L_2(\xi)d\xi\right)\\
S_{L_2}(\phi) &= \exp\left(-\sum_{i=E}^{L_2}\frac{n_i}{\alpha_i} - k\int_{\hat{\phi}_{E:L_2}}^{\hat{\phi}_{L_1:L_2}} \ln\left(1-\frac{u}{k}W(\phi)\right)d\xi - n_C\int_{\hat{\phi}_{L_1:L_2}}^{\hat{\phi}_{L_2:L_2}} L_1(\xi)+\psi L_2(\xi)d\xi\right.\\
&\quad \left. -n_C\int_{\hat{\phi}_{L_2:L_2}}^{\phi} L_1(\xi)/\psi+L_2(\xi)d\xi\right)\\
S_P(\phi) &= \exp\left(-\sum_{i=E}^{P}\frac{n_i}{\alpha_i} - k\int_{\hat{\phi}_{E:P}}^{\hat{\phi}_{L_1:P}} \ln\left(1-\frac{u}{k}W(\phi)\right)d\xi - n_C\int_{\hat{\phi}_{L_1:P}}^{\hat{\phi}_{L_2:P}} L_1(\xi)+\psi L_2(\xi)d\xi\right.\\
&\quad \left. -n_C\int_{\hat{\phi}_{L_2:P}}^{\hat{\phi}_{P:P}} L_1(\xi)/\psi+L_2(\xi)d\xi\right)\\
S_Pw(\phi) &= \exp\left(-\sum_{i=L_1}^{P}\frac{n_i}{\alpha_i} - n_C\int_{\hat{\phi}_{L_1:P}}^{\hat{\phi}_{L_2:P}} L_1(\xi)+\psi L_2(\xi)d\xi - n_C\int_{\hat{\phi}_{L_2:P}}^{\hat{\phi}_{P:P}} L_1(\xi)/\psi+L_2(\xi)d\xi\right)
\end{aligned}
$$

Figure C8 shows the predicted dynamics as a function of the birth rate scalar, search efficiency and interference among wasps.

## Model I: Parasitism

$$
\begin{aligned}
\frac{dE(\phi)}{d\phi} &= cA(\phi) - cA(\phi_E)S_E(\phi) - \left(n_E + k\ln\left(1-\frac{u}{k}W(\phi)\right)\right)E(\phi)\\
\frac{dA(\phi)}{d\phi} &= cA(\phi_P)S_P(\phi) - n_A A(\phi)\\
\frac{dW(\phi)}{d\phi} &= k\ln\left(1-\frac{u}{k}W(\phi_P)\right)E(\phi_P)S_Pw - n_W W(\phi)\\
S_E(\phi) &= \exp\left(-\frac{n_E}{\alpha_E} - k\int_{\hat{\phi}_{E:E}}^{\phi}\ln\left(1-\frac{u}{k}W(\phi)\right)d\xi\right)\\
S_P(\phi) &= \exp\left(-\sum_{i=E}^{P}\frac{n_i}{\alpha_i} - k\int_{\hat{\phi}_{E:P}}^{\hat{\phi}_{L_1:P}}\ln\left(1-\frac{u}{k}W(\phi)\right)d\xi\right)\\
S_Pw(\phi) &= \exp\left(-\sum_{i=L_1}^{P}\frac{n_i}{\alpha_i}\right)
\end{aligned}
$$

Figure C9 shows the predicted dynamics as a function of the birth rate scalar, search efficiency and interference among wasps.

## Model J: Symmetric larval density-dependence with winter mortality

$$
\begin{aligned}
\frac{dE(\phi)}{d\phi} &= cA(\phi) - cA(\phi_E)S_E(\phi) - \left(n_E + n_{q_1}\frac{e^{-n_{q_2}m(\phi)}}{m(\phi)}\right)E(\phi)\\
\frac{dL_1(\phi)}{d\phi} &= cA(\phi_E)S_E(\phi) - cA(\phi_{L_1})S_{L_1}(\phi) - (n_L + n_C L(\phi))\,L_1(\phi)\\
\frac{dL_2(\phi)}{d\phi} &= cA(\phi_{L_1})S_{L_1}(\phi) - cA(\phi_{L_2})S_{L_2}(\phi) - (n_L + n_C L(\phi))\,L_2(\phi)\\
\frac{dP(\phi)}{d\phi} &= cA(\phi_{L_2})S_{L_2}(\phi) - cA(\phi_P)S_P(\phi) - \left(n_P + n_{q_1}\frac{e^{-n_{q_2}m(\phi)}}{m(\phi)}\right)P(\phi)\\
\frac{dA(\phi)}{d\phi} &= cA(\phi_P)S_P(\phi) - \left(n_A + n_{q_1}\frac{e^{-n_{q_2}m(\phi)}}{m(\phi)}\right)A(\phi)\\
S_E(\phi) &= \exp\left(-\frac{n_E}{\alpha_E} - n_{q_1}\int_{\hat{\phi}_{E:E}}^{\phi}\frac{e^{-n_{q_2}m(\xi)}}{m(\xi)}d\xi\right)\\
S_{L_1}(\phi) &= \exp\left(-\sum_{i=E}^{L_1}\frac{n_i}{\alpha_i} - n_{q_1}\int_{\hat{\phi}_{E:L_1}}^{\hat{\phi}_{L_1:L_1}}\frac{e^{-n_{q_2}m(\xi)}}{m(\xi)}d\xi - n_C\int_{\hat{\phi}_{L_1:L_1}}^{\phi}L(\xi)d\xi\right)\\
S_{L_2}(\phi) &= \exp\left(-\sum_{i=E}^{L_2}\frac{n_i}{\alpha_i} - n_{q_1}\int_{\hat{\phi}_{E:L_2}}^{\hat{\phi}_{L_1:L_2}}\frac{e^{-n_{q_2}m(\xi)}}{m(\xi)}d\xi - n_C\int_{\hat{\phi}_{L_1:L_2}}^{\phi}L(\xi)d\xi\right)\\
S_P(\phi) &= \exp\left(-\sum_{i=E}^{P}\frac{n_i}{\alpha_i} - n_{q_1}\int_{\hat{\phi}_{E:P}}^{\hat{\phi}_{L_1:P}}\frac{e^{-n_{q_2}m(\xi)}}{m(\xi)}d\xi - n_C\int_{\hat{\phi}_{L_1:P}}^{\hat{\phi}_{P:P}}L(\xi)d\xi - n_{q_1}\int_{\hat{\phi}_{P:P}}^{\phi}\frac{e^{-n_{q_2}m(\xi)}}{m(\xi)}d\xi\right)
\end{aligned}
$$

where $L(\phi) = L_1(\phi) + L_2(\phi)$. Figure C10 shows the predicted dynamics as a function with a realistic temperature driver.

## Model K: Symmetrical larval competition with senescence and winter mortality

$$
\begin{aligned}
\frac{dE(\phi)}{d\phi} &= cA(\phi) - cA(\phi_E)S_E(\phi) - \left(n_E + n_{q_1}\frac{e^{-n_{q_2}m(\phi)}}{m(\phi)}\right)E(\phi)\\
\frac{dL_1(\phi)}{d\phi} &= cA(\phi_E)S_E(\phi) - cA(\phi_{L_1})S_{L_1}(\phi) - (n_L + n_C L(\phi))\,L_1(\phi)\\
\frac{dL_2(\phi)}{d\phi} &= cA(\phi_{L_1})S_{L_1}(\phi) - cA(\phi_{L_2})S_{L_2}(\phi) - (n_L + n_C L(\phi))\,L_2(\phi)\\
\frac{dP(\phi)}{d\phi} &= cA(\phi_{L_2})S_{L_2}(\phi) - cA(\phi_P)S_P(\phi) - \left(n_P + n_{q_1}\frac{e^{-n_{q_2}m(\phi)}}{m(\phi)}\right)P(\phi)\\
\frac{dA(\phi)}{d\phi} &= cA(\phi_P)S_P(\phi) - cA(\phi_A)S_A(\phi) - \left(n_A + n_{q_1}\frac{e^{-n_{q_2}m(\phi)}}{m(\phi)}\right)A(\phi)\\
S_E(\phi) &= \exp\left(-\frac{n_E}{\alpha_E} - n_{q_1}\int_{\hat{\phi}_{E:E}}^{\phi}\frac{e^{-n_{q_2}m(\xi)}}{m(\xi)}d\xi\right)\\
S_{L_1}(\phi) &= \exp\left(-\sum_{i=E}^{L_1}\frac{n_i}{\alpha_i} - n_{q_1}\int_{\hat{\phi}_{E:L_1}}^{\hat{\phi}_{L_1:L_1}}\frac{e^{-n_{q_2}m(\xi)}}{m(\xi)}d\xi - n_C\int_{\hat{\phi}_{L_1:L_1}}^{\phi}L(\xi)d\xi\right)\\
S_{L_2}(\phi) &= \exp\left(-\sum_{i=E}^{L_2}\frac{n_i}{\alpha_i} - n_{q_1}\int_{\hat{\phi}_{E:L_2}}^{\hat{\phi}_{L_1:L_2}}\frac{e^{-n_{q_2}m(\xi)}}{m(\xi)}d\xi - n_C\int_{\hat{\phi}_{L_1:L_2}}^{\phi}L(\xi)d\xi\right)\\
S_P(\phi) &= \exp\left(-\sum_{i=E}^{P}\frac{n_i}{\alpha_i} - n_{q_1}\int_{\hat{\phi}_{E:P}}^{\hat{\phi}_{L_1:P}}\frac{e^{-n_{q_2}m(\xi)}}{m(\xi)}d\xi - n_C\int_{\hat{\phi}_{L_1:P}}^{\hat{\phi}_{P:P}}L(\xi)d\xi - n_{q_1}\int_{\hat{\phi}_{P:P}}^{\phi}\frac{e^{-n_{q_2}m(\xi)}}{m(\xi)}d\xi\right)\\
S_A(\phi) &= \exp\left(-\sum_{i=E}^{A}\frac{n_i}{\alpha_i} - n_{q_1}\int_{\hat{\phi}_{E:A}}^{\hat{\phi}_{L_1:A}}\frac{e^{-n_{q_2}m(\xi)}}{m(\xi)}d\xi - n_C\int_{\hat{\phi}_{L_1:A}}^{\hat{\phi}_{P:A}}L(\xi)d\xi - n_{q_1}\int_{\hat{\phi}_{P:A}}^{\phi}\frac{e^{-n_{q_2}m(\xi)}}{m(\xi)}d\xi\right)
\end{aligned}
$$

where $L(\phi) = L_1(\phi) + L_2(\phi)$. Figure C11 shows the predicted dynamics as a function with a realistic temperature driver.

## Model L: Symmetrical larval competition with Allee effect and winter mortality

$$\frac{dE(\phi)}{d\phi} = c\left(1 - e^{\nu A(\phi)}\right) A(\phi) - c\left(1 - e^{\nu A(\phi_E)}\right) A(\phi_E) S_E(\phi) - \left(n_E + n_{q_1} \frac{e^{-n_{q_2} m(\phi)}}{m(\phi)}\right) E(\phi)$$

$$\frac{dL_1(\phi)}{d\phi} = c\left(1 - e^{\nu A(\phi_E)}\right) A(\phi_E) S_E(\phi) - c\left(1 - e^{\nu A(\phi_{L_1})}\right) A(\phi_{L_1}) S_{L_1}(\phi) - (n_L + n_C L(\phi))\, L_1(\phi)$$

$$\frac{dL_2(\phi)}{d\phi} = c\left(1 - e^{\nu A(\phi_{L_1})}\right) A(\phi_{L_1}) S_{L_1}(\phi) - c\left(1 - e^{\nu A(\phi_{L_2})}\right) A(\phi_{L_2}) S_{L_2}(\phi) - (n_L + n_C L(\phi))\, L_2(\phi)$$

$$\frac{dP(\phi)}{d\phi} = c\left(1 - e^{\nu A(\phi_{L_2})}\right) A(\phi_{L_2}) S_{L_2}(\phi) - c\left(1 - e^{\nu A(\phi_P)}\right) A(\phi_P) S_P(\phi) - \left(n_P + n_{q_1} \frac{e^{-n_{q_2} m(\phi)}}{m(\phi)}\right) P(\phi)$$

$$\frac{dA(\phi)}{d\phi} = c\left(1 - e^{\nu A(\phi_P)}\right) A(\phi_P) S_P(\phi) - \left(n_A + n_{q_1} \frac{e^{-n_{q_2} m(\phi)}}{m(\phi)}\right) A(\phi)$$

$$S_E(\phi) = \exp\left(-\frac{n_E}{\alpha_E} - n_{q_1} \int_{\hat{\phi}_{E:E}}^{\phi} \frac{e^{-n_{q_2} m(\xi)}}{m(\xi)} d\xi\right)$$

$$S_{L_1}(\phi) = \exp\left(-\sum_{i=E}^{L_1} \frac{n_i}{\alpha_i} - n_{q_1} \int_{\hat{\phi}_{E:L_1}}^{\hat{\phi}_{L_1:L_1}} \frac{e^{-n_{q_2} m(\xi)}}{m(\xi)} d\xi - n_C \int_{\hat{\phi}_{L_1:L_1}}^{\phi} L(\xi) d\xi\right)$$

$$S_{L_2}(\phi) = \exp\left(-\sum_{i=E}^{L_2} \frac{n_i}{\alpha_i} - n_{q_1} \int_{\hat{\phi}_{E:L_2}}^{\hat{\phi}_{L_1:L_2}} \frac{e^{-n_{q_2} m(\xi)}}{m(\xi)} d\xi - n_C \int_{\hat{\phi}_{L_1:L_2}}^{\phi} L(\xi) d\xi\right)$$

$$S_P(\phi) = \exp\left(-\sum_{i=E}^{P} \frac{n_i}{\alpha_i} - n_{q_1} \int_{\hat{\phi}_{E:P}}^{\hat{\phi}_{L_1:P}} \frac{e^{-n_{q_2} m(\xi)}}{m(\xi)} d\xi - n_C \int_{\hat{\phi}_{L_1:P}}^{\hat{\phi}_{P:P}} L(\xi) d\xi - n_{q_1} \int_{\hat{\phi}_{P:P}}^{\phi} \frac{e^{-n_{q_2} m(\xi)}}{m(\xi)} d\xi\right)$$

where $L(\phi) = L_1(\phi) + L_2(\phi)$. Figure C12 shows the predicted dynamics as a function with a realistic temperature driver.

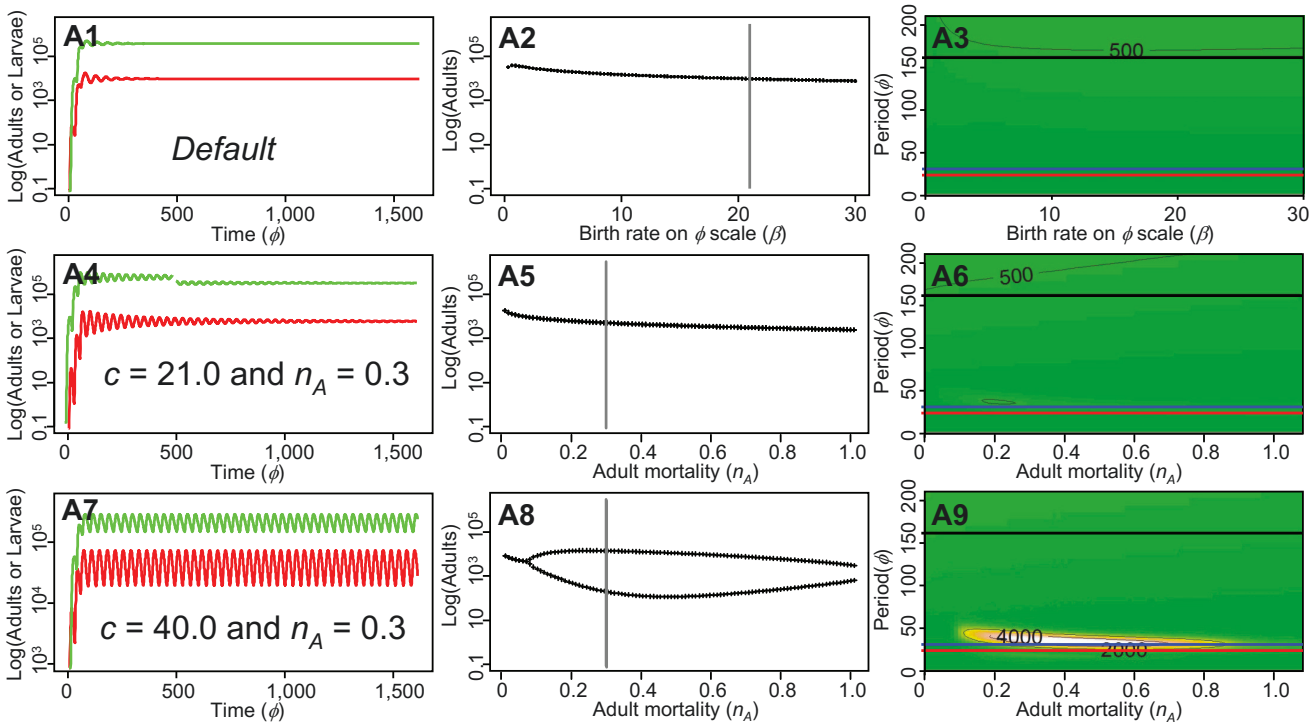


**Figure C1.** Illustrative model dynamics for Model A. Left hand panel shows adult (red) and larval (green) dynamics, middle panel is the bifurcation plot showing the maximum and minimum of adult abundance as a function of a model parameter, and right panel is a color map of the the corresponding periodiogram. The vertical gray line in the middle panel indicates parameter location for the simulation in the left panel, and parameters other than those given are in Table 2. Horizontal lines on the periodiogram are the reference lines from Figure 2. Each row illustrates the change in dynamics as a function of a model parameter.

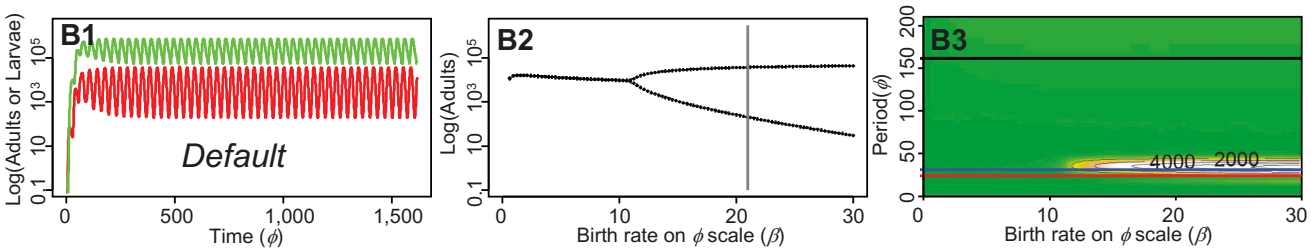


**Figure C2.** Illustrative model dynamics for Model B. See Figure C1 for legend details.

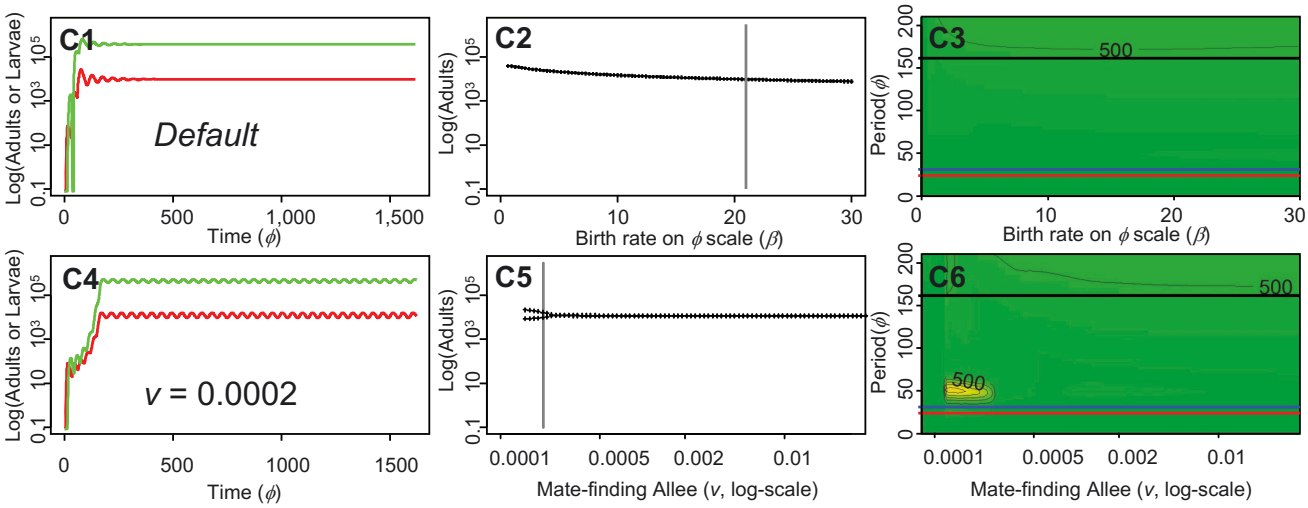


**Figure C3.** Illustrative model dynamics for Model C. See Figure C1 for legend details.

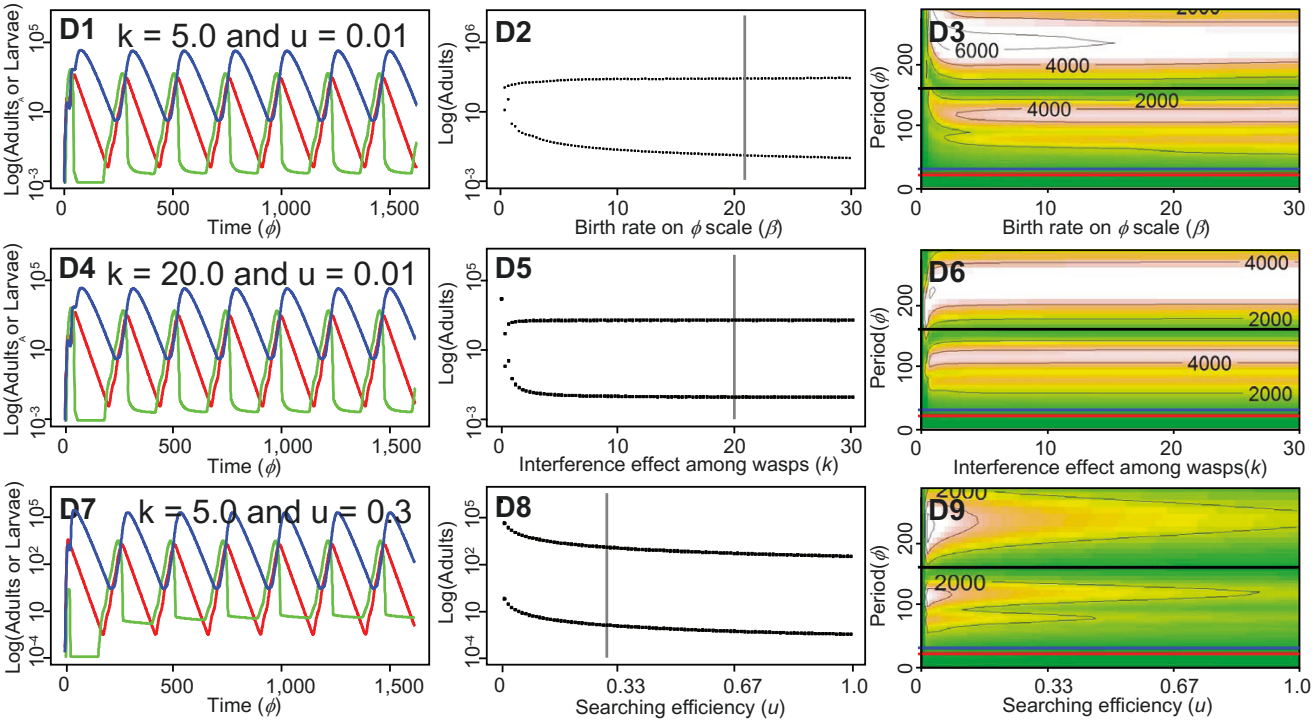


**Figure C4.** Illustrative model dynamics for Model D. See Figure C1 for legend details.

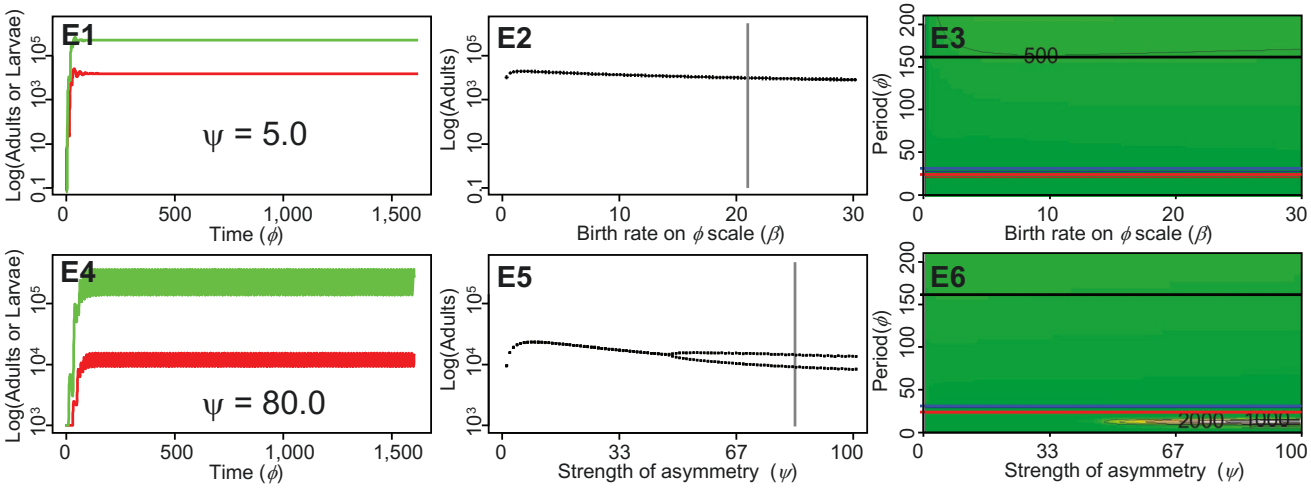


**Figure C5.** Illustrative model dynamics for Model E. See Figure C1 for legend details.

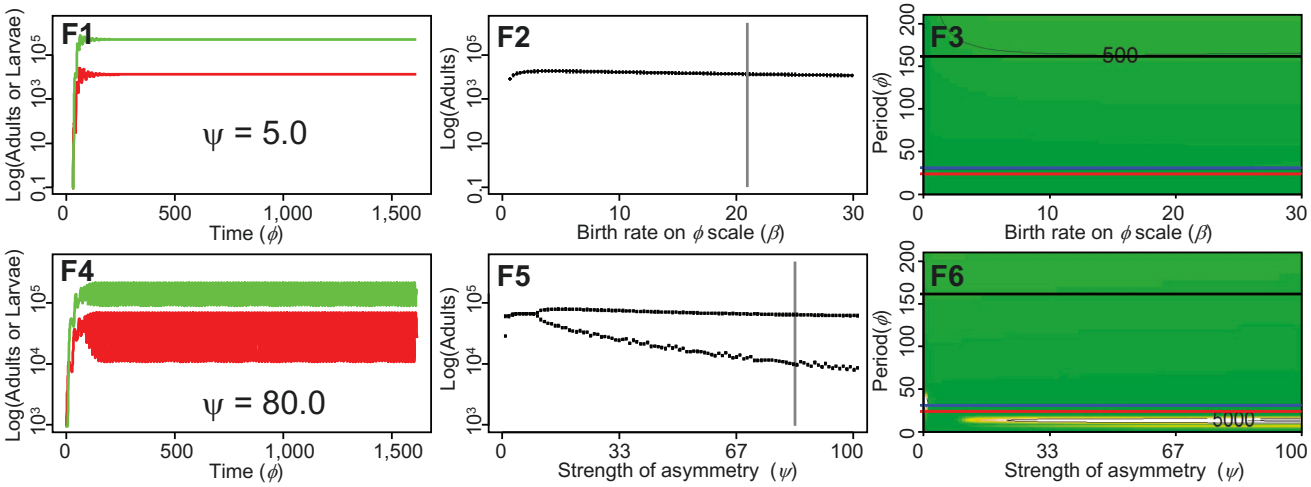


**Figure C6.** Illustrative model dynamics for Model F. See Figure C1 for legend details.

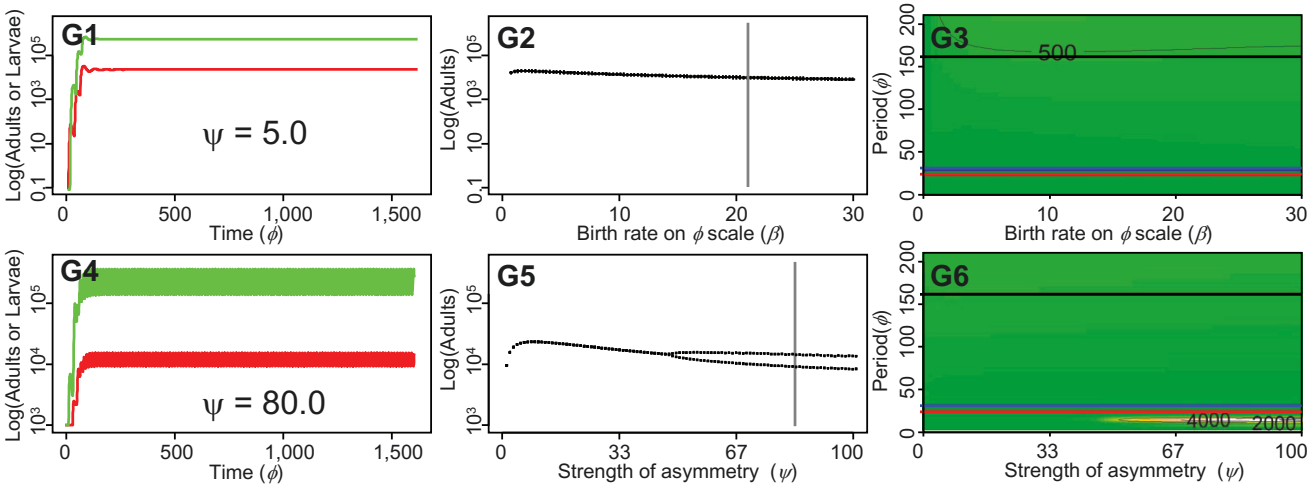


**Figure C7.** Illustrative model dynamics for Model G. See Figure C1 for legend details.

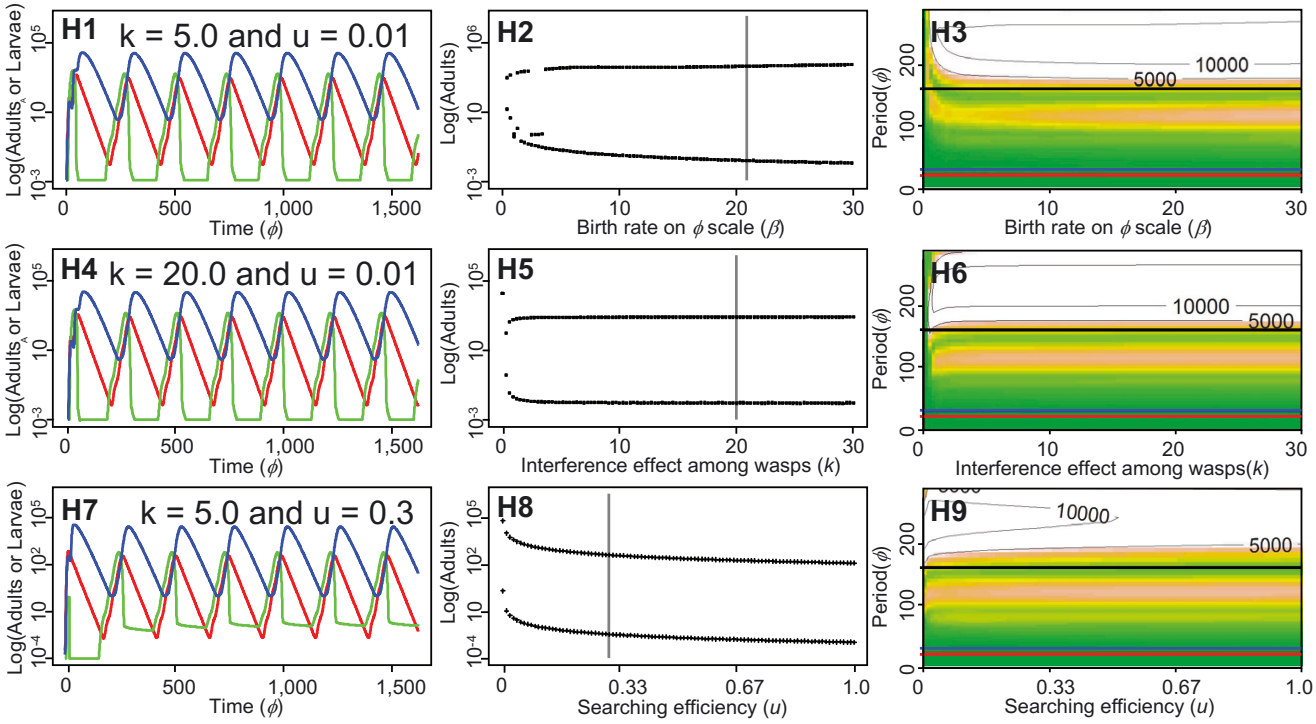


**Figure C8.** Illustrative model dynamics for Model H. See Figure C1 for legend details.

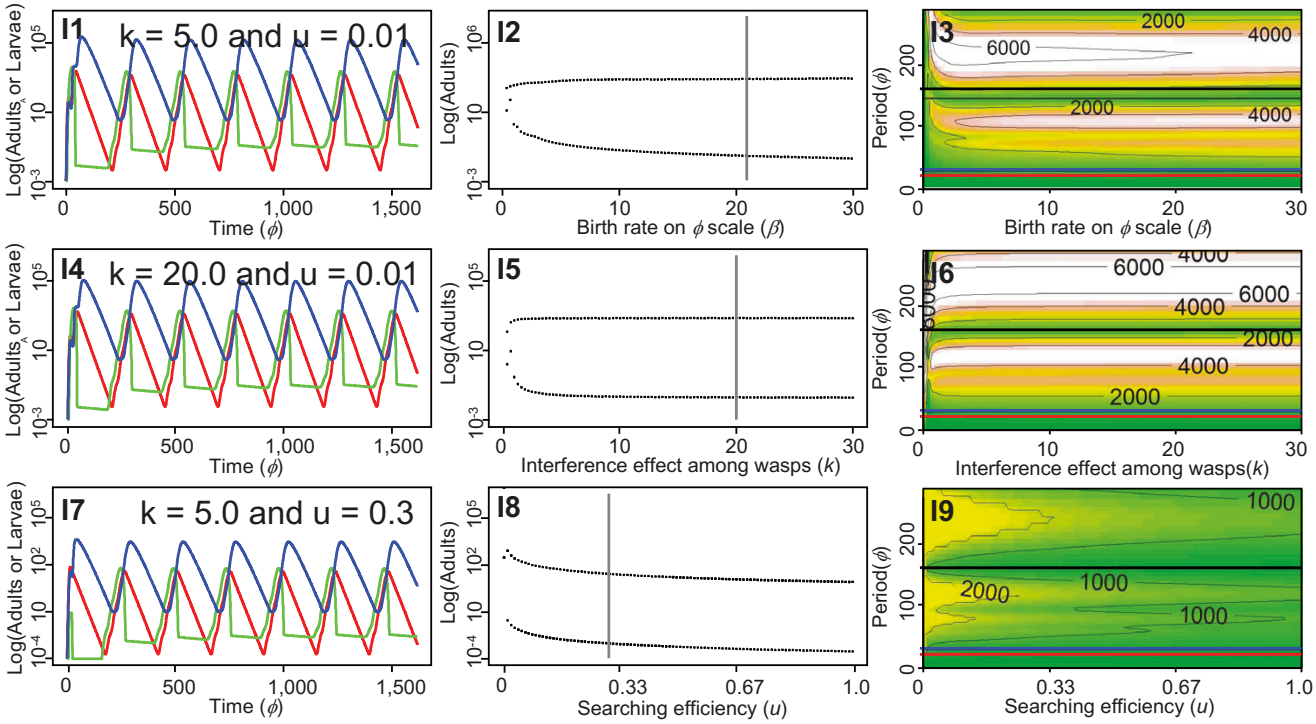


**Figure C9.** Illustrative model dynamics for Model I. See Figure C1 for legend details.

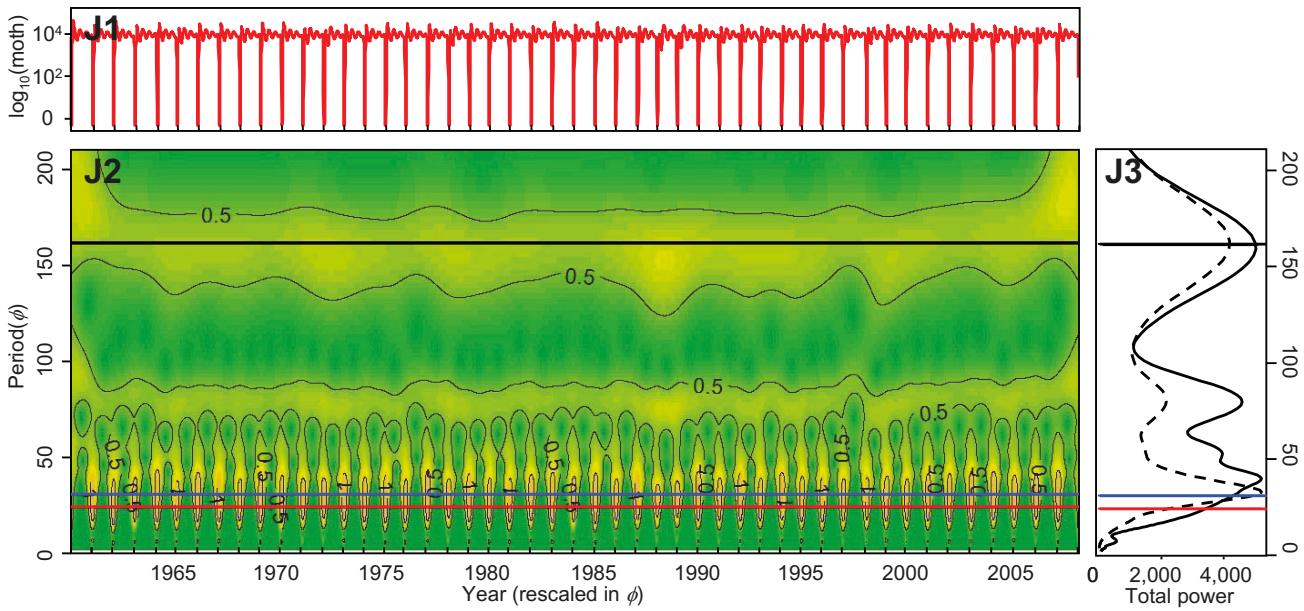


**Figure C10.** Illustrative model dynamics for Model J. See Figure C1 for legend details.

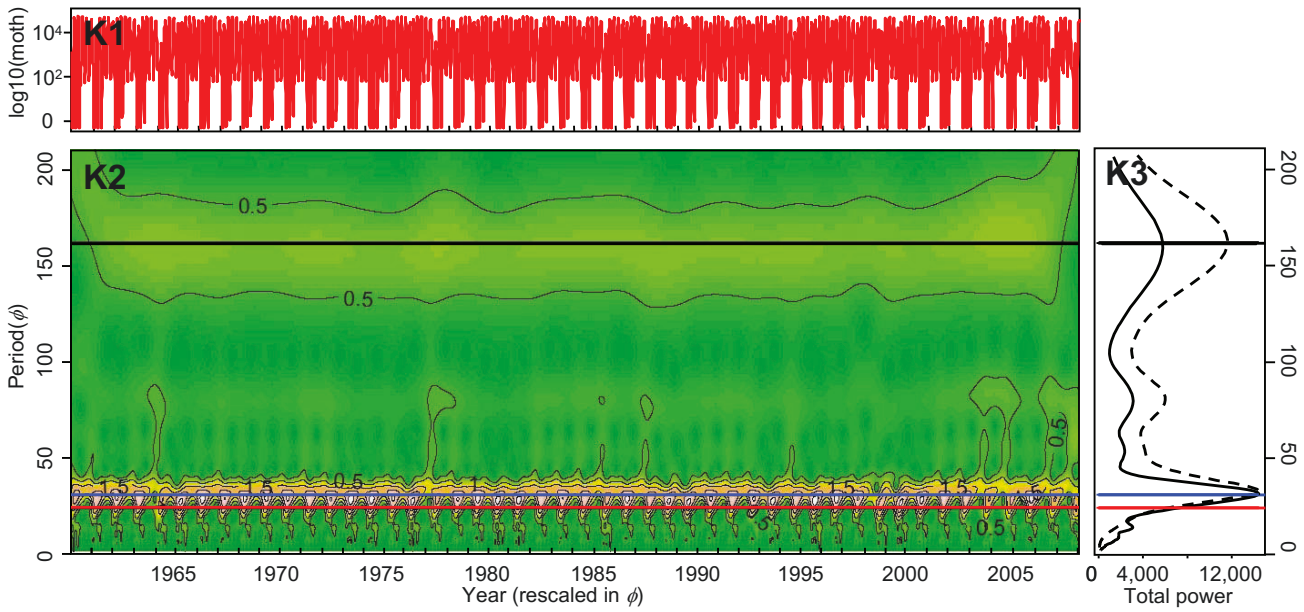


**Figure C11.** Illustrative model dynamics for Model K. See Figure C1 for legend details.

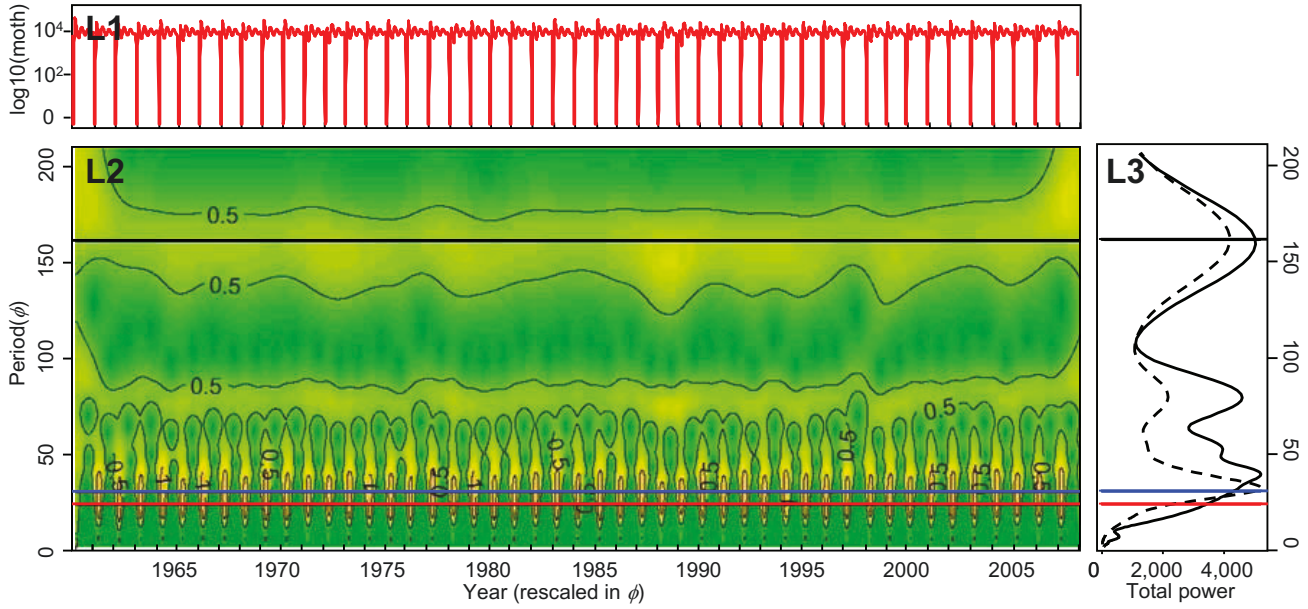


**Figure C12.** Illustrative model dynamics for Model L. See Figure C1 for legend details.

## Appendix D: Model robustness to variation in stage development rates

To assess the robustness of single-generation cycles in the fixed-delay model (Appendix B) to realistic variation in stage development rates, we develop a variant of the model with distributed stage durations. To construct the model, we assume that the delays in each stage are Gamma-distributed with and integer shape parameter, which is equivalent to dividing each stage into $n$ substages, each with exponentially distributed substage duration. Following from Appendix B, the dynamics of each stage can be rewritten as

$$\frac{dC_{i,1}(\phi)}{d\phi} = n\alpha_{i-1}C_{i-1,n}(\phi) - n\alpha_i C_{i,1}(\phi) - \frac{\delta_i(\phi)}{m(\phi)}C_{i,1}(\phi) \tag{D1}$$

$$\frac{dC_{i,j}(\phi)}{d\phi} = n\alpha_i \left(C_{i,j-1}(\phi) - C_{i,j}(\phi)\right) - \frac{\delta_i(\phi)}{m(\phi)}C_{i,j}(\phi) \tag{D2}$$

where $C_{i,j}$ is the density of individuals in substage $j$ of stage $i$. If $i = 1$, then $n\alpha_{i-1}C_{i-1,n}(\phi)$ is the birth rate $\beta(\phi)/m(\phi)$. Nabeta et al. (2005) report the standard error ($SE$) and sample size $x$ for the egg, larvae and pupae stage durations. We convert these numbers to estimates of standard deviations on the time-scale using $\sigma = SE\sqrt{x}$. The egg stage had a higher variance ($\sigma_E^2 = 3.2$) than the larvae ($\sigma_L^2 = 1.0$) or pupae stage ($\sigma_P^2 = 0.6$). However, the influence of development rate variation on single-generation cycles in the model was not symmetric. We found that variance in the larvae, pupae and adult development rates had a large impact on the presence of limit cycles, but variance in the egg stage had no influence, so the remaining analyses are based on the variance in the larvae and pupae stages only. To compare the observed variation with the variation in the distributed delay model, we transformed the observed variance from the time-scale to the phi-scale using $\sigma^2(\phi) = \sigma^2(t)(g(t)^2)$ , and calculate the scale ($\kappa$) and shape ($\theta$) parameters of a Gamma distribution using the expected larval stage duration using the data of 20 °C from Appendix A and the variance ($\kappa = 0.055$, $\theta = 247.3$). The empirical distribution of stage durations corresponds to the distribution of stage durations predicted by the distributed delay model with roughly 200 substages (Figure C1), which has the same single-generation cycles as the fixed-delay model.

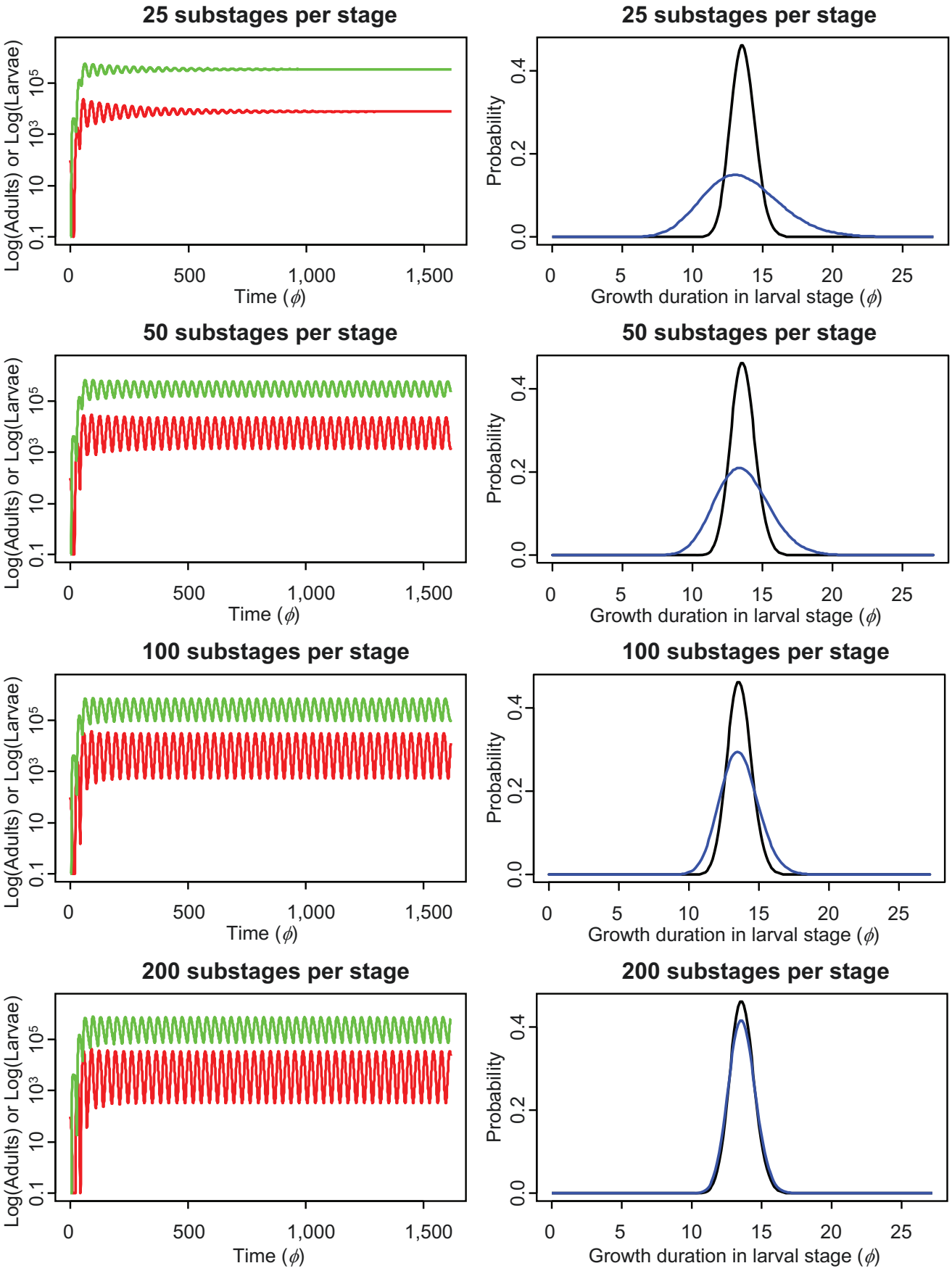


**Figure D1.** Influence of development rate variation on single-generation cycles. The left panels show population dynamics of larvae (green lines) and adult (red lines) of the model with adult senescence and without winter hardiness (corresponding to Figure 3a). Right panels show the variation in the growth duration of the larval stage. Results are shown for $n$ =25, 50, 100, and 200 (blue lines). Observed variation in stage durations (dotted lines) corresponds to a distributed delay model with 200 substages per stage, which has the same dynamics as the point delay model.